From bloodjournal.hematologylibrary.org at KYOTO UNIVERSITY on March 26, 2012. For personal use only.

type 1 diabetes[49] and chronic graft-versus-host disease.[50] These findings suggest that proteasome inhibitors may be exploited for the treatment of these autoimmune or inflammatory disorders through their suppressive activity on pDCs. The second generation of proteasome inhibitors that have less neurotoxicity than bortezomib and are thus more suitable for long-term use may be applicable to such chronic inflammatory disorders.

In conclusion, the results of this study suggest that bortezomib suppresses the activity of pDCs by disrupting the coordinated trafficking of nucleic acid-sensing TLRs and Unc93B1 from the ER to endolysosomes and by suppressing the UPR. Bortezomib or a next generation of proteasome inhibitors may therefore be instrumental in treating pDC-mediated, IFN-α-driven inflammatory disorders.

Acknowledgments

We thank Millennium Pharmaceuticals for providing bortezomib, Dr Reiko Saito for providing influenza virus, and Keiko Fukunaga for her excellent technical assistance.

This study was supported by research funding from Ministry of Education, Culture, Sports, Science, and Technology of Japan (17016034).

Authorship

Contribution: M.H. performed research and cowrote the manuscript; N.K. designed research, analyzed and interpreted data, and cowrote the manuscript; T.K. contributed vital experimental designs and techniques; H.F. performed research; A.T.-K. contributed vital experimental designs and techniques; R.F. and K.M. contributed vital analytical tools; T.M. and S.K. contributed vital new reagents; and Y.M. and T.U. supervised the whole project.

Conflict-of-interest disclosure: The authors declare no competing financial interests.

Correspondence: Norimitsu Kadowaki, Department of Hematology and Oncology, Graduate School of Medicine, Kyoto University, 54 Shogoin Kawara-cho, Sakyo-ku, Kyoto 606-8507, Japan; e-mail: kadowaki@kuhp.kyoto-u.ac.jp.

References

1. Banchereau J, Briere F, Caux C, et al. Immunobiology of dendritic cells. *Annu Rev Immunol.* 2000; 18(1):767-811.
2. Liu YJ, Kanzler H, Soumelis V, Gilliet M. Dendritic cell lineage, plasticity and cross-regulation. *Nat Immunol.* 2001;2(7):585-589.
3. Kadowaki N, Ho S, Antonenko S, et al. Subsets of human dendritic cell precursors express different Toll-like receptors and respond to different microbial antigens. *J Exp Med.* 2001;194(6):863-870.
4. Liu YJ. IPC: professional type 1 interferon-producing cells and plasmacytoid dendritic cell precursors. *Annu Rev Immunol.* 2005;23(1):275-306.
5. Swiecki M, Colonna M. Unraveling the functions of plasmacytoid dendritic cells during viral infections, autoimmunity, and tolerance. *Immunol Rev.* 2010;234(1):142-162.
6. Gilliet M, Cao W, Liu YJ. Plasmacytoid dendritic cells: sensing nucleic acids in viral infection and autoimmune diseases. *Nat Rev Immunol.* 2008; 8(8):594-606.
7. Rönnblom L, Alm GV. A pivotal role for the natural interferon alpha-producing cells (plasmacytoid dendritic cells) in the pathogenesis of lupus. *J Exp Med.* 2001;194(12):F59-F63.
8. Barrat FJ, Meeker T, Gregorio J, et al. Nucleic acids of mammalian origin can act as endogenous ligands for Toll-like receptors and may promote systemic lupus erythematosus. *J Exp Med.* 2005;202(8):1131-1139.
9. Vollmer J, Tluk S, Schmitz C, et al. Immune stimulation mediated by autoantigen binding sites within small nuclear RNAs involves Toll-like receptors 7 and 8. *J Exp Med.* 2005;202(11):1575-1585.
10. Blanco P, Palucka AK, Gill M, Pascual V, Banchereau J. Induction of dendritic cell differentiation by IFN-alpha in systemic lupus erythematosus. *Science.* 2001;294(5546):1540-1543.
11. Bennett L, Palucka AK, Arce E, et al. Interferon and granulopoiesis signatures in systemic lupus erythematosus blood. *J Exp Med.* 2003;197(6): 711-723.
12. Lande R, Gregorio J, Facchinetti V, et al. Plasmacytoid dendritic cells sense self-DNA coupled with antimicrobial peptide. *Nature.* 2007;449(7162): 564-569.
13. Ganguly D, Chamilos G, Lande R, et al. Self-RNA-antimicrobial peptide complexes activate human dendritic cells through TLR7 and TLR8. *J Exp Med.* 2009;206(9):1983-1994.
14. Iwakoshi NN, Pypaert M, Glimcher LH. The transcription factor XBP1 is essential for the development and survival of dendritic cells. *J Exp Med.* 2007;204(10):2267-2275.
15. Todd DJ, Lee AH, Glimcher LH. The endoplasmic reticulum stress response in immunity and autoimmunity. *Nat Rev Immunol.* 2008;8(9):663-674.
16. Lee A-H, Iwakoshi NN, Glimcher LH. XBP1 regulates a subset of endoplasmic reticulum resident chaperone genes in the unfolded protein response. *Mol Cell Biol.* 2003;23(21):7448-7459.
17. Shaffer AL, Shapiro-Shelef M, Iwakoshi NN, et al. XBP1, downstream of Blimp-1, expands the secretory apparatus and other organelles, and increases protein synthesis in plasma cell differentiation. *Immunity.* 2004;21(1):81-93.
18. Latz E, Schoenemeyer A, Visintin A, et al. TLR9 signals after translocating from the ER to CpG DNA in the lysosome. *Nat Immunol.* 2004;5(2): 190-198.
19. Brinkmann MM, Spooner E, Hoebe K, Beutler B, Ploegh HL, Kim YM. The interaction between the ER membrane protein UNC93B and TLR3, 7, and 9 is crucial for TLR signaling. *J Cell Biol.* 2007; 177(2):265-275.
20. Kim YM, Brinkmann MM, Paquet ME, Ploegh HL. UNC93B1 delivers nucleotide-sensing toll-like receptors to endolysosomes. *Nature.* 2008; 452(7184):234-238.
21. Richardson PG, Mitsiades C, Hideshima T, Anderson KC. Bortezomib: proteasome inhibition as an effective anticancer therapy. *Annu Rev Med.* 2006;57(1):33-47.
22. Lee AH, Iwakoshi NN, Anderson KC, Glimcher LH. Proteasome inhibitors disrupt the unfolded protein response in myeloma cells. *Proc Natl Acad Sci U S A.* 2003;100(17):9946-9951.
23. Obeng EA, Carlson LM, Gutman DM, Harrington WJ, Jr., Lee KP, Boise LH. Proteasome inhibitors induce a terminal unfolded protein response in multiple myeloma cells. *Blood.* 2006;107(12): 4907-4916.
24. Reimold AM, Iwakoshi NN, Manis J, et al. Plasma cell differentiation requires the transcription factor XBP1. *Nature.* 2001;412(6844):300-307.
25. Iwakoshi NN, Lee A-H, Vallabhajosyula P, Otipoby KL, Rajewsky K, Glimcher LH. Plasma cell differentiation and the unfolded protein response intersect at the transcription factor XBP1. *Nat Immunol.* 2003;4(4):321-329.
26. Carrasco DR, Sukhdeo K, Protopopova M, et al. The differentiation and stress response factor XBP1 drives multiple myeloma pathogenesis. *Cancer Cell.* 2007;11(4):349-360.
27. Mancini R, Fagioli C, Fra AM, Maggioni C, Sitia R. Degradation of unassembled soluble Ig subunits by cytosolic proteasomes: evidence that retrotranslocation and degradation are coupled events. *FASEB J.* 2000;14(5):769-778.
28. Grouard G, Rissoan MC, Filgueira L, Durand I, Banchereau J, Liu YJ. The enigmatic plasmacytoid T cells develop into dendritic cells with interleukin (IL)-3 and CD40-ligand. *J Exp Med.* 1997; 185(6):1101-1111.
29. Maeda T, Murata K, Fukushima T, et al. A novel plasmacytoid dendritic cell line, CAL-1, established from a patient with blastic natural killer cell lymphoma. *Int J Hematol.* 2005;81(2):148-154.
30. Kawamura K, Kadowaki N, Kitawaki T, Uchiyama T. Virus-stimulated plasmacytoid dendritic cells induce CD4+ cytotoxic regulatory T cells. *Blood.* 2006;107(3):1031-1038.
31. Krug A, Rothenfusser S, Hornung V, et al. Identification of CpG oligonucleotide sequences with high induction of IFN-alpha/beta in plasmacytoid dendritic cells. *Eur J Immunol.* 2001;31(7):2154-2163.
32. Takahashi K, Shibata T, Akashi-Takamura S, et al. A protein associated with Toll-like receptor (TLR) 4 (PRAT4A) is required for TLR-dependent immune responses. *J Exp Med.* 2007;204(12): 2963-2976.
33. Fukui R, Saitoh S, Matsumoto F, et al. Unc93B1 biases Toll-like receptor responses to nucleic acid in dendritic cells toward DNA- but against RNA-sensing. *J Exp Med.* 2009;206(6):1339-1350.
34. Krieg AM, Yi AK, Matson S, et al. CpG motifs in bacterial DNA trigger direct B-cell activation. *Nature.* 1995;374(6522):546-549.
35. Papandreou CN, Daliani DD, Nix D, et al. Phase I trial of the proteasome inhibitor bortezomib in patients with advanced solid tumors with observations in androgen-independent prostate cancer. *J Clin Oncol.* 2004;22(11):2108-2121.
36. Ogawa Y, Tobinai K, Ogura M, et al. Phase I and II pharmacokinetic and pharmacodynamic study of the proteasome inhibitor bortezomib in Japanese patients with relapsed or refractory multiple myeloma. *Cancer Sci.* 2008;99(1):140-144.

From bloodjournal.hematologylibrary.org at KYOTO UNIVERSITY on March 26, 2012. For personal use only.

37. Blanco B, Perez-Simon JA, Sanchez-Abarca LI, et al. Bortezomib induces selective depletion of alloreactive T lymphocytes and decreases the production of Th1 cytokines. *Blood.* 2006;107(9): 3575-3583.
38. Dzionek A, Fuchs A, Schmidt P, et al. BDCA-2, BDCA-3, and BDCA-4: three markers for distinct subsets of dendritic cells in human peripheral blood. *J Immunol.* 2000;165(11):6037-6046.
39. Kadowaki N, Antonenko S, Lau JY, Liu YJ. Natural interferon alpha/beta-producing cells link innate and adaptive immunity. *J Exp Med.* 2000; 192(2):219-226.
40. Kaisho T, Tanaka T. Turning NF-κB and IRFs on and off in DC. *Trends Immunol.* 2008;29(7):329-336.
41. Kukreja A, Hutchinson A, Mazumder A, et al. Bortezomib disrupts tumour-dendritic cell interactions in myeloma and lymphoma: therapeutic implications. *Br J Haematol.* 2007;136(1):106-110.
42. Chauhan D, Singh AV, Brahmandam M, et al. Functional interaction of plasmacytoid dendritic cells with multiple myeloma cells: a therapeutic target. *Cancer Cell.* 2009;16(4):309-323.
43. Lee AH, Chu GC, Iwakoshi NN, Glimcher LH. XBP1 is required for biogenesis of cellular secretory machinery of exocrine glands. *EMBO J.* 2005;24(24):4368-4380.
44. Honda K, Yanai H, Negishi H, et al. IRF-7 is the master regulator of type-I interferon-dependent immune responses. *Nature.* 2005;434(7034):772-777.
45. Fribley A, Zeng Q, Wang CY. Proteasome inhibitor PS-341 induces apoptosis through induction of endoplasmic reticulum stress-reactive oxygen species in head and neck squamous cell carcinoma cells. *Mol Cell Biol.* 2004;24(22):9695-9704.
46. Nawrocki ST, Carew JS, Pino MS, et al. Bortezomib sensitizes pancreatic cancer cells to endoplasmic reticulum stress-mediated apoptosis. *Cancer Res.* 2005;65(24):11658-11666.
47. Banchereau J, Pascual V. Type I interferon in systemic lupus erythematosus and other autoimmune diseases. *Immunity.* 2006;25(3):383-392.
48. Kono DH, Haraldsson MK, Lawson BR, et al. Endosomal TLR signaling is required for anti-nucleic acid and rheumatoid factor autoantibodies in lupus. *Proc Natl Acad Sci U S A.* 2009;106(29): 12061-12066.
49. Li Q, Xu B, Michie SA, Rubins KH, Schreriber RD, McDevitt HO. Interferon-alpha initiates type 1 diabetes in nonobese diabetic mice. *Proc Natl Acad Sci U S A.* 2008;105(34):12439-12444.
50. Imanguli MM, Swaim WD, League SC, Gress RE, Pavletic SZ, Hakim FT. Increased T-bet+ cytotoxic effectors and type I interferon-mediated processes in chronic graft-versus-host disease of the oral mucosa. *Blood.* 2009;113(15):3620-3630.

British Journal of Cancer (2011) 104, 91 – 100
© 2011 Cancer Research UK All rights reserved 0007 – 0920/11
www.bjcancer.com

Antiproliferative and proapoptotic activity of GUT-70 mediated through potent inhibition of Hsp90 in mantle cell lymphoma

L Jin[1,2], Y Tabe[*,1], S Kimura[3], Y Zhou[1], J Kuroda[4], H Asou[5], T Inaba[5], M Konopleva[6], M Andreeff[7] and T Miida[1]

[1]Department of Clinical Laboratory Medicine, Juntendo University School of Medicine, 2-1-1 Hongo, Bunkyo-ku, Tokyo 113-8421, Japan; [2]Sportology Center, Juntendo University School of Medicine, 2-1-1 Hongo, Bunkyo-ku, Tokyo 113-8421, Japan; [3]Division of Hematology, Respiratory Medicine and Oncology, Department of Internal Medicine, Faculty of Medicine, Saga University, 5-1-1 Nabeshima, Saga 849-8501, Japan; [4]Division of Hematology and Oncology, Department of Medicine, Kyoto Prefectural University of Medicine, 465 Kajii-cho, Kamigyo-ku, Kyoto 602-8566, Japan; [5]Department of Molecular Oncology and Leukemia Program Project, Research Institute for Radiation Biology & Medicine, Hiroshima University, 1-2-3 Kasumi, Minami-ku, Hiroshima 734-8553, Japan; [6]Department of Leukemia, The University of Texas MD Anderson Cancer Center, 1515 Holcombe Blvd., Houston, TX 77030, USA; [7]Department of Stem Cell Transplantation and Cellular Therapy, The University of Texas MD Anderson Cancer Center, 1515 Holcombe Blvd., Houston, TX 77030, USA

BACKGROUND: Mantle cell lymphoma (MCL) is an aggressive B-cell lymphoma with poor prognosis, requiring novel anticancer strategies.

METHODS: Mantle cell lymphoma cell lines with known *p53* status were treated with GUT-70, a tricyclic coumarin derived from *Calophyllum brasiliense*, and the biological and biochemical consequences of GUT-70 were studied.

RESULTS: GUT-70 markedly reduced cell proliferation/viability through G_1 cell cycle arrest and increased apoptosis, with greater sensitivity in mutant (mt)-*p53*-expressing MCL cells than in wild-type (wt)-*p53*-bearing cells. Mechanistically, GUT-70 showed binding affinity to heat-shock protein 90 (Hsp90) and ubiquitin-dependent proteasomal degradation of Hsp90 client proteins, including cyclin D1, Raf-1, Akt, and mt-p53. Depletion of constitutively overexpressed cyclin D1 by GUT-70 was accompanied by p27 accumulation and decreased Rb phosphorylation. GUT-70 induced mitochondrial apoptosis with Noxa upregulation and Mcl-1 downregulation in mt-*p53* cells, but Mcl-1 accumulation in wt-*p53* cells. Noxa and Mcl-1 were coimmunoprecipitated, and activated BAK. Treatment with a combination of GUT-70 and bortezomib or doxorubicin had synergistic antiproliferative effects in MCL cells that were independent of *p53* status.

CONCLUSION: GUT-70 has pronounced antiproliferative effects in MCL with mt-*p53*, a known negative prognostic factor for MCL, through Hsp90 inhibition. These findings suggest that GUT-70 has potential utility for the treatment of MCL.

British Journal of Cancer (2011) **104,** 91 – 100. doi:10.1038/sj.bjc.6606007 www.bjcancer.com
Published online 7 December 2010
© 2011 Cancer Research UK

Keywords: GUT-70; mantle cell lymphoma; apoptosis; p53; Hsp90; coumarin

Mantle cell lymphoma (MCL) is characterised by an aggressive clinical course, with rapid relapse after an initial response or primary resistance to standard chemotherapy (Jares *et al*, 2007). The t(11,14)(q13;32) translocation of MCL leads to overexpression of cyclin D1, which is believed to be associated with oncogenesis by causing instability of the G_1/S checkpoint through promotion of cyclin-dependent kinase activity and through sequestration of the Cip/Kip family of cyclin-dependent kinase inhibitors (Sherr and Roberts, 1999; Quintanilla-Martinez *et al*, 2003). These activities facilitate phosphorylation and inactivation of the retinoblastoma (Rb) G_1/S checkpoint protein, resulting in cell cycle progression. It has been demonstrated, however, that overexpression of cyclin D1 itself is not sufficient for development of MCL, suggesting that additional genetic events might be necessary for oncogenesis (Bodrug *et al*, 1994), particularly as apoptosis-related genes such as *p53*, *INK4a/ARF*, and *ATM* are dysregulated in MCL (Fernàndez *et al*, 2005; Greiner *et al*, 2006).

In MCL, mutation/overexpression of *p53* is reported as an adverse prognostic indicator (Jares *et al*, 2007). As many of the antitumour effects mediated by chemotherapeutic agents depend on a *p53*-related pathway, resistance to chemotherapy often develops through impaired *p53* signalling (Döhner *et al*, 1995). The 26S proteasome inhibitor bortezomib retains activity in *p53*-mutant (mt-*p53*) cells and has demonstrated single-agent efficacy in relapsed or refractory MCL, which is, however, based mainly on prolonged response rather than on an increase in ultimate survival rate (Goy *et al*, 2009).

Therefore, development of novel compounds that target *p53*-independent signalling pathways is of considerable interest in the treatment of this disease.

We have reported that the newly discovered anticancer agent GUT-70, a natural product derived from the stem bark of *Calophyllum brasiliense*, demonstrated cytotoxic efficacy in human leukaemic cells (Kimura *et al*, 2005). GUT-70 (Figure 1), characterised as a tricyclic coumarin with the formula

*Correspondence: Dr Y Tabe; E-mail: tabe@juntendo.ac.jp
Revised 6 October 2010; accepted 22 October 2010; published online 7 December 2010

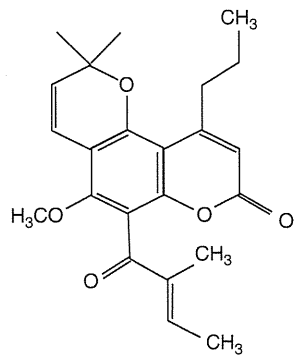

Figure 1 Chemical structure of GUT-70.

5-methoxy-2,2-dimethyl-6-(2-methyl-1-oxo-2-butenyl) -10-propyl-2*H*,8*H*-benzo[1,2-*b*;3,4-*b*']dipyran-8-one ($C_{23}H_{26}O_5$), significantly inhibited leukaemic cell growth with a median inhibitory concentration (IC_{50}) of 2-5 μM without repressing colony formation by normal haematopoietic progenitors or proliferation of normal human hepatocytes at concentrations up to 30 μM (Kimura *et al*, 2005).

Coumarin antibiotics have been reported to bind the newly discovered C-terminal ATP binding site of 90 kDa heat-shock protein (Hsp90), a molecular chaperone responsible for the folding and conformational maintenance of client proteins (Marcu *et al*, 2000; Issacs *et al*, 2003; Pratt and Toft, 2003; Donnelly *et al*, 2008). Hsp90 inhibition results in degradation of misfolded Hsp90 clients through ubiquitination, followed by proteasome-mediated hydrolysis (Zhang *et al*, 2004). As many of the Hsp90 client proteins contribute to cancer cell proliferation, Hsp90 has emerged as a promising target for cancer chemotherapy (Issacs *et al*, 2003; Donnelly *et al*, 2008).

In this study, GUT-70 demonstrated antiproliferative and proapoptotic activities with more prominent efficacy in mt-*p53*-bearing MCL cells than in those with wild-type (wt) *p53*. GUT-70 showed binding affinity to Hsp90, and reduced expression of Hsp90 client proteins such as mt-p53, Raf-1, cyclin D1, and Akt. The intrinsic apoptotic pathway was activated by GUT-70 through upregulation of Noxa and BAK activation. The combination of GUT-70 with bortezomib or doxorubicin yielded synergistic antiproliferative effects independent of *p53* status. These findings indicate possible efficacy and a rationale for further exploration of GUT-70 as a new therapeutic strategy for MCL.

MATERIALS AND METHODS

Cell lines and culture conditions

Four MCL cell lines were used in this study: JVM-2 (Melo *et al*, 1986), Granta 519 (Jadayel *et al*, 1997) and MINO (Lai *et al*, 2002) were kindly provided by Dr M Raffeld, and Jeko-1 (Raynaud *et al*, 1993) was a gift from Dr M Seto. Granta 519 and JVM-2 express wt-*p53*, whereas Jeko-1 and MINO express *p53* mutations (Jeko-1, loss of *p53* expression; MINO, mutation at codon 147 (valine→glycine)) (Raynaud *et al*, 1993; Lai *et al*, 2002). JVM-2, Jeko-1 and MINO were cultured in RPMI 1640 medium containing 15% fetal bovine serum (FBS) and 1% penicillin/streptomycin. Granta 519 was grown in Dulbecco's modified Eagle's medium (DMEM) supplemented with 15% FBS. Cells were first acclimated in RPMI 1640 or DMEM containing 5% FBS for 16 h before exposure to GUT-70 (Nippon Shinyaku, Kyoto, Japan) (Kimura *et al*, 2005). Control cells were treated with an equivalent amount of dimethyl sulphoxide (DMSO). Doxorubicin was obtained from Sigma (St Louis, MO, USA) and bortezomib was provided by Millennium (Cambridge, MA, USA). Human osteosarcoma cell line U2OS transfected with the histone cluster 1 (*H2BK*) and enhanced green fluorescent protein (*EGFP*) genes, U2OS-H2BK-EGFP, was grown in DMEM supplemented with 10% FBS and used for morphological observation. U2OS expresses wt-*p53* (Flørenes *et al*, 1994).

Cell viability/proliferation assay

Cell viability was assessed by the Trypan blue dye exclusion method, and cell proliferation was determined by the CellTiter 96 AQueous One Solution Cell Proliferation Assay (MTS; Promega, Madison, WI, USA).

Apoptosis analysis

Apoptotic cell death was evaluated through annexin V (Roche Diagnostic, Indianapolis, IN, USA) and propidium iodide (PI) positivities by a FACScan flow cytometer and Cell Quest software (Becton Dickinson Immunocytometry Systems, San Jose, CA, USA). The extent of drug-specific apoptosis was assessed by the following formula: % specific apoptosis = (test−control) × 100/(100−control).

Flow cytometric analysis of cell cycle and BAK activation

Cell cycle distribution was determined by flow cytometric analysis of PI-stained nuclei. DNA content was determined by FACScan flow cytometer and CellQuest software. BAK activation was analyzed as previously described (Samraj *et al*, 2006). Briefly, cells were fixed and permeabilized using the DAKO IntraStain kit (DakoCytomation, Glostrup, Denmark) according to the manufacturer's instructions. Cells were then stained with conformation-specific monoclonal antibody against BAK (y164; Abcam, Cambridge, MA, USA) or isotype-matched control antibody for 30 min at room temperature, followed by incubation with Alexafluor 488-labeled chicken anti-rabbit secondary antibody (Molecular Probes, Eugene, OR, USA) for 30 min on ice in the dark. After the washing step, conformational change of BAK was analyzed by a FACScan flow cytometer.

Western blot analysis and immunoprecipitation

Cells were solubilised in lysis buffer (phosphate-buffered saline solution (PBS), 1 × cell lysis buffer (Cell Signaling Technology, Danvers, MA, USA), 1 × protease inhibitor (Roche), and 1 × phosphatase inhibitor cocktails I and II (Calbiochem, San Diego, CA, USA)), and incubated for 30 min on ice. Total protein (20 μg) was separated by sodium dodecyl sulphate polyacrylamide gel electrophoresis (SDS-PAGE), immunoblotted with appropriate antibodies, and reacted with enhanced chemiluminescence reagent (Amersham Biosciences, Piscataway, NJ, USA); signals were detected by a luminescent image analyser (LAS-1000 plus; Fujifilm, Tokyo, Japan). The anti-α-tubulin or anti-β-actin blot was used in parallel as a loading control. For immunoblotting, the following antibodies were used: $p21^{Cip1/WAF1}$, $p27^{KIP1}$, and Mcl-1 (BD-Pharmingen, San Diego, CA, USA); p53 (DO-7; Dako, Carpinteria, CA, USA); Noxa (Calbiochem); α-tubulin (Sigma-Aldrich, St Louis, MO, USA); Puma (Upstate Biotechnology, Lake Placid, NY, USA); LC-3 (MBL, Nagoya, Japan); ubiquitin (Santa Cruz Biotechnology, Santa Cruz, CA, USA); and Hsp70, c-Raf, Akt, ERK1/2, phosphorylated-ERK1/2 $^{Thr202/Tyr204}$(p-ERK1/2), cyclin D1, phosphorylated Rb^{Ser780} (p-Rb), Bim, BAK, cleaved caspase-9, cleaved caspase-3, β-actin, and horseradish peroxidase-linked anti-mouse and anti-rabbit IgG (all from Cell Signaling Technology). Protein lysates were subjected to immunoprecipitation using anti-Mcl-1 (Santa Cruz Biotechnology).

© 2011 Cancer Research UK

Hsp90 binding assay

The Hsp90α inhibitor screening assay kit with Hsp90α recombinant enzyme and fluorescein isothiocyanate (FITC)-labelled geldanamycin was used (BPS Bioscience, San Diego, CA, USA). The competition of fluorescence-labelled geldanamycin for binding to purified recombinant Hsp90α was measured by Flex Station 3 (Molecular Devices, Sunnyvale, CA, USA).

Morphological observation

U2OS-H2BK-EGFP cells (2.0×10^5 per ml) were cultured in a 35-mm dish and treated with 5 μM GUT-70 or DMSO only. Each dish was placed on the stage of a light microscope equipped with a digital camera (BZ-8000; Keyence, Osaka, Japan) at 37 °C under a humidified atmosphere of 5% CO_2. Video images were collected over the period from 12 to 48 h after treatment.

mRNA quantification by real-time reverse-transcriptase PCR (RT-PCR)

Total RNAs were extracted from cells with the RNeasy Mini Kit (Qiagen, Hilden, Germany). First-strand cDNA synthesis was performed with oligo(dT) as primer (Superscript II System; Invitrogen, Carlsbad, CA, USA). Real-time reverse-transcriptase PCR was performed by the Model 7500 Real-time PCR System (Applied Biosystems, Foster City, CA, USA). Expression of *Noxa* and *GAPDH* mRNA was detected by TaqMan Gene Expression Assays (*Noxa*: Hs00560402_m1, *GAPDH*: Hs99999905_m1; Applied Biosystems). The PCR cycle number that generated the first

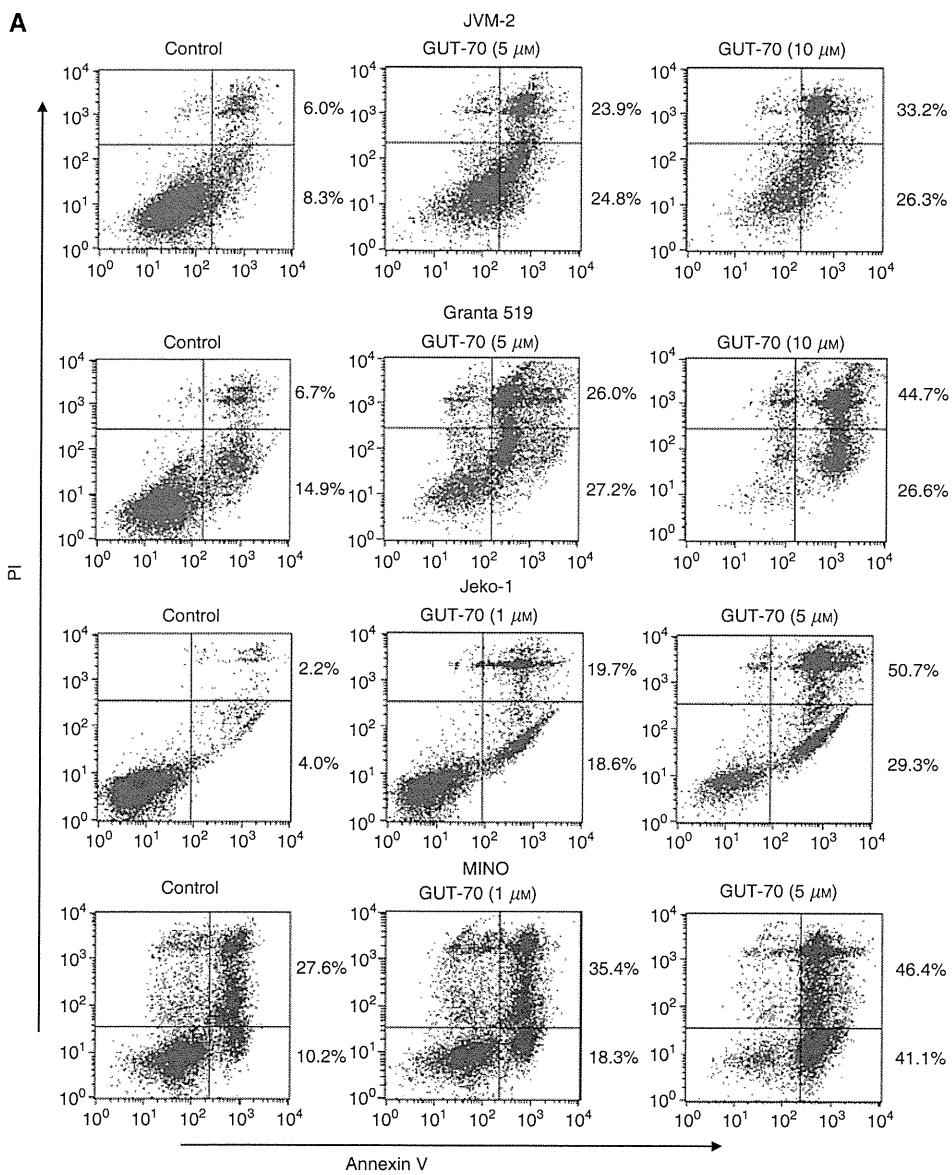

Figure 2 GUT-70-induced cell growth inhibition, apoptosis, and cell cycle arrest in MCL. (**A**) JVM-2, Granta 519, Jeko-1, and MINO cells were treated with the indicated concentrations of GUT-70 for 48 h, and the percentages of apoptotic cells were quantified by annexin V/PI staining. (**B**) Representative flow cytometric histograms of PI-treated cells after 24 h of GUT-70 treatment at indicated concentrations. The percentages of G_0/G_1-, S- and G_2/M-phase cells were assessed in total viable cells (bar graphs).

© 2011 Cancer Research UK

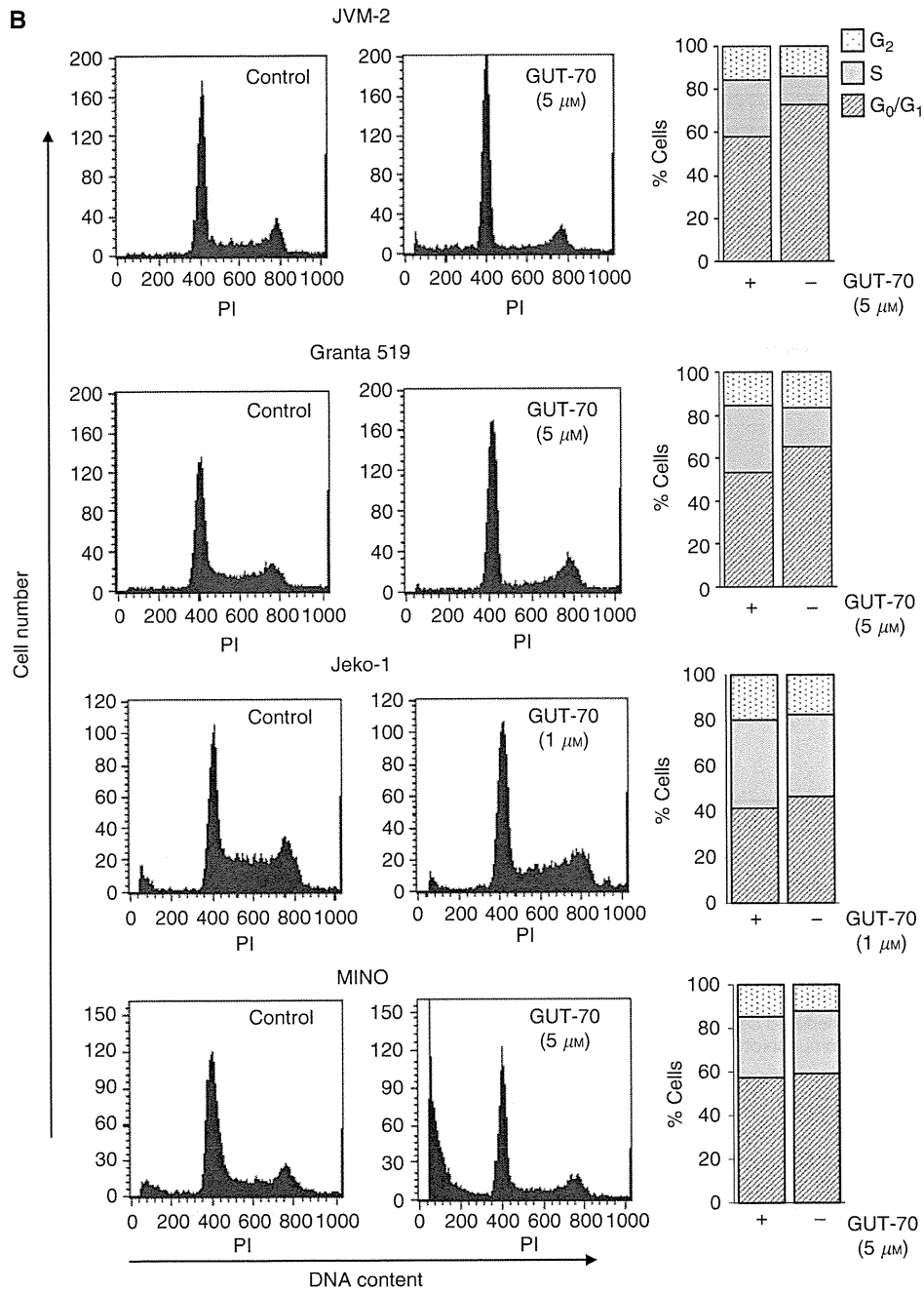

Figure 2 Continued.

fluorescence signal above a threshold value (the threshold cycle; C_t) was determined. The abundance of each transcript of *Noxa* relative to that of *GAPDH* was calculated as follows: relative expression $= 100 \times 2$ exp $[-\Delta C_t]$, where ΔC_t is the mean C_t of the transcript of interest minus the mean C_t of the transcript for *GAPDH*. The C_t data from duplicate PCRs were averaged for calculation of relative expression.

Statistical analysis

Cytotoxicity was assessed by the Chou-Talalay method (Chou and Talalay, 1984) using Calcusyn software (Biosoft, Cambridge, UK). The combination index (CI) values indicate degree of synergism: strong synergism (0.3–0.7), moderate synergism (0.7–0.85), and slight synergism (0.85–0.9).

RESULTS

GUT-70 induces apoptosis and cell cycle arrest in MCL cells

Treatment with GUT-70 (Figure 1) for 48 h resulted in dose-dependent cell growth inhibition detected by MTS cell proliferation assay (IC_{50}: Granta 519, 6. 3 μM; JVM-2, 4.5 μM; Jeko-1, 1.7 μM; MINO, 1.5 μM).

To determine whether the inhibition of cell growth by GUT-70 was associated with apoptosis and/or cell cycle arrest, we

© 2011 Cancer Research UK

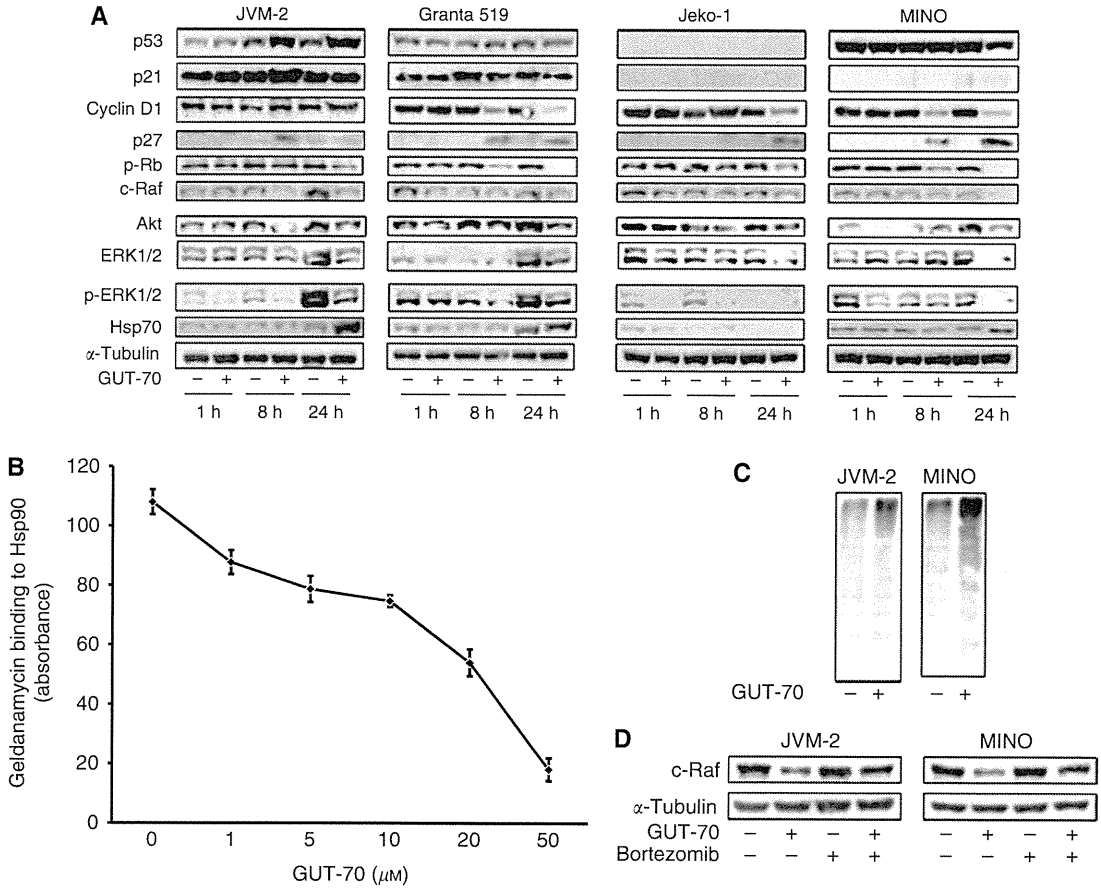

Figure 3 (**A**) GUT-70 effects on Hsp90 client proteins. MCL cells were treated with GUT-70 (JVM-2, 5 μM; Granta 519, 5 μM; Jeko-1, 1 μM; MINO, 5 μM) for indicated times. Cells were subjected to lysis and analysed by western blot. Western blot images are representative results from three independent experiments. (**B**) GUT-70 competitively inhibited geldanamycin binding to the Hsp90α subunit. The competition of GUT-70 with FITC-labelled geldanamycin for binding to purified recombinant Hsp90α was measured. Fluorescence was measured at λex 485 nm and at λem 525 nm. Results shown are means ± s.d. from three independent experiments. (**C**) GUT-70 induced protein ubiquitination. JVM-2 and MINO cells were treated with 5 μM GUT-70 for 24 h, subjected to lysis, and immunoblotted for ubiquitin. Representative results are shown from three independent experiments. (**D**) Proteasome inhibitor bortezomib prevented GUT-70-mediated decreased expression of c-Raf. JVM-2 and MINO cells were treated with 5 μM GUT-70 and/or 10 nM bortezomib for 24 h, subjected to lysis, and immunoblotted for c-Raf. Western blot images are representative results from three independent experiments.

conducted flow cytometric analysis of annexin V/PI-stained and PI-stained nuclei. As shown in Figure 2A, 48 h of GUT-70 treatment induced dose-dependent increases of annexin V positivity in all cell lines; this effect was more pronounced in mt-*p53*-bearing Jeko-1 and MINO cells than in wt-*p53*-bearing Granta 519 and JVM-2 cells (specific apoptosis by 5 μM GUT-70: 40.3% for Granta 519, 40.1% for JVM-2, 78.8% for Jeko-1, 79.9% for MINO). The PI cell cycle histograms further demonstrated that GUT-70 increased the sub-G_1 fraction in a time-dependent manner at a lower dose for mt-*p53* cells than for wt-*p53* cells; sub-G_1 fractions at 24 and 48 h were 4.6 and 10.7% for Granta 519 (5 μM GUT-70), 14.8 and 34.7% for JVM-2 (5 μM), 5.2 and 19.3% for Jeko-1 (1 μM), and 12.0 and 34.9% for MINO (1 μM). Whereas GUT-70 impeded G_1-S cell cycle progression in JVM-2 and Granta 519 cells, G_1-S arrest was minimal in MINO and Jeko-1 cells (Figure 2B). These data suggest that GUT-70-induced cell growth inhibition resulted in part from cell cycle arrest at the G_0/G_1 checkpoint and in part from apoptosis induction.

GUT-70 downregulates mutated p53 and cyclin D1 and accumulates p27

We next investigated changes in cell cycle regulatory proteins associated with GUT-70 treatment. As shown in Figure 3A, GUT-70 induced p53/p21 accumulation in JVM-2 cells, but did not increase p53/p21 expression in Granta 519 cells. In Jeko-1 cells, basal p53/p21 expression was not detectable and was unaffected by GUT-70. Notably, expression of the overexpressed mt-p53 protein was reduced in MINO cells by 24 h exposure to GUT-70, without detectable p21 expression. The expression level of p27 was upregulated by GUT-70, irrespective of *p53* status. GUT-70 diminished the highly expressed cyclin D1 in all tested MCL cells except JVM-2, and resulted in substantial decreases in Rb phosphorylation in all tested cells (Figure 3).

GUT-70 induces degradation of Hsp90 substrate proteins

The coumarin antibiotics have been reported to bind to Hsp90 (Marcu *et al*, 2000). To investigate whether GUT-70 has binding affinity for Hsp90, a competitive binding assay was performed using geldanamycin, a well-characterised ATP competitive inhibitor (Gooljarsingh *et al*, 2006). GUT-70 demonstrated dose-dependent inhibition of geldanamycin binding to Hsp90, which indicated the binding activity of GUT-70 to Hsp90 (Figure 3B). The degradation by GUT-70 of Hsp90 client proteins, such as Raf-1 and its downstream ERK1/2 and phospho ERK1/2, as well as Akt (Pratt and Toft, 2003; Zhang *et al*, 2004, 2005), was detected by

© 2011 Cancer Research UK

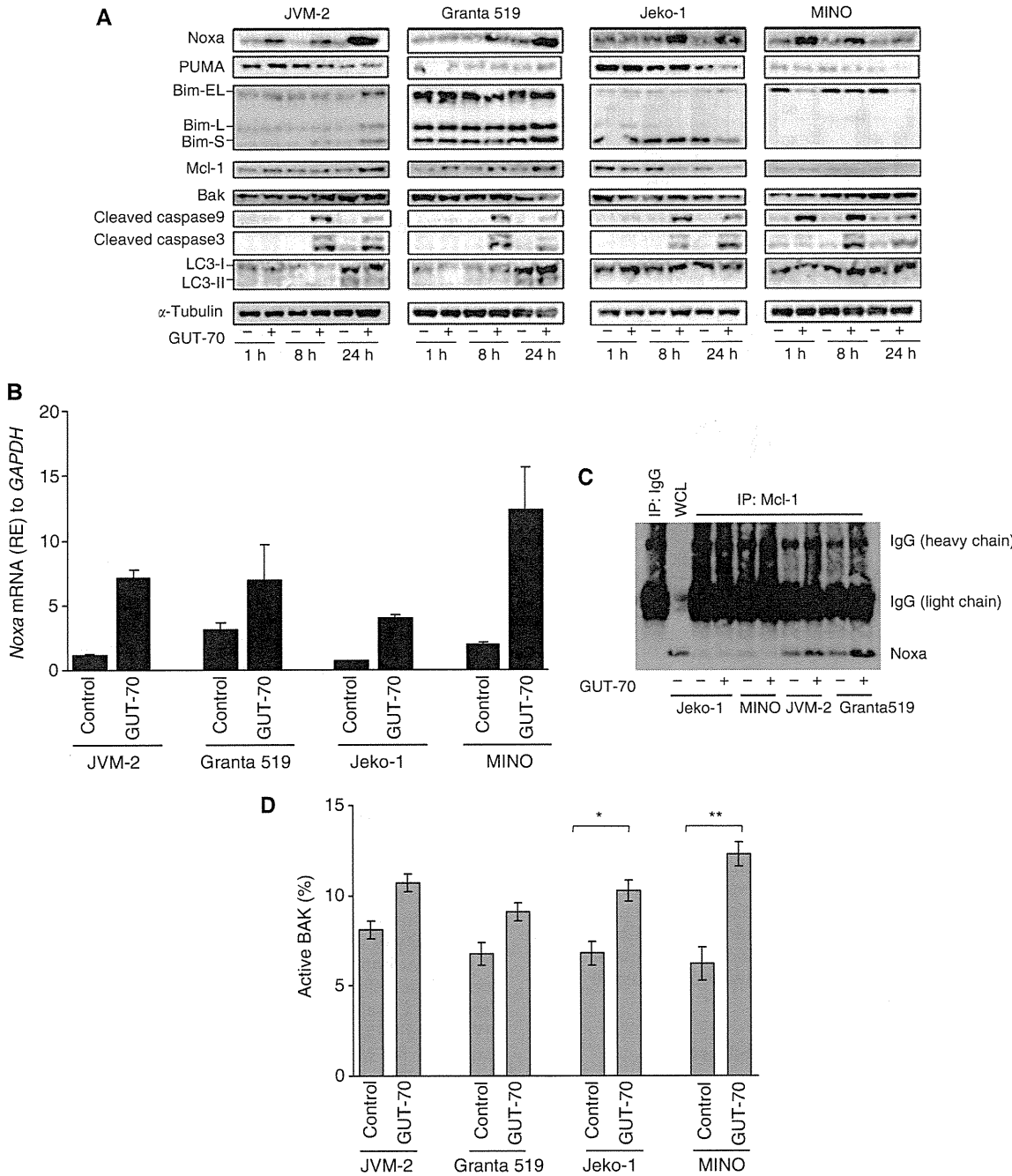

Figure 4 Modulation of apoptosis-related protein levels by GUT-70. MCL cells were treated with GUT-70 (JVM-2, 5 μM; Granta 519, 5 μM; Jeko-1, 1 μM; MINO, 5 μM) for the indicated times. (**A**) Cells were subjected to lysis, then apoptosis-related proteins and macroautophagy marker LC3 were analysed by western blot. Western blot images are representative results from three independent experiments. (**B**) Cells were harvested after 18 h treatment with GUT-70, and *Noxa* mRNA expression levels were detected by TaqMan RT–PCR analysis. The abundance of transcripts of *Noxa* relative to *GAPDH* transcripts was determined as described in Materials and Methods. Graphs show the representative data from two independent experiments with similar results. (**C**) Cells were treated with GUT-70 for 24 h, and Mcl-1 immunoprecipitation was performed as described in Materials and Methods. Total extracts were analysed by western blotting for Noxa. Western blot images are representative results from three independent experiments. (**D**) Cells were treated with GUT-70 for 24 h, then conformational changes in BAK were measured by intracellular flow cytometry as described in Materials and methods. To block the caspase activation-mediated conformational changes of BAK, cells were preincubated for 1 h with 100 μM Z-VAD-FMK. Data represent duplicate experiments. $^{*}P<0.01$; $^{**}P<0.05$. RE, relative expression.

western blot analysis in all tested MCL cells (Figure 3A). Cyclin D1 and mt-p53, the expression of which was repressed by GUT-70, are known substrate proteins of Hsp90 (Zhang *et al*, 2004; Muller *et al*, 2008). Furthermore, GUT-70 increased expression of Hsp70, a marker of Hsp90 inhibition (Elo *et al*, 2005; Bao *et al*, 2009), in Granta 519, JVM-2, and MINO cells. In Jeko-1 cells, however, Hsp70 was detected at a level insufficient to be reliable as a marker without further induction by GUT-70 (Figure 3A).

© 2011 Cancer Research UK

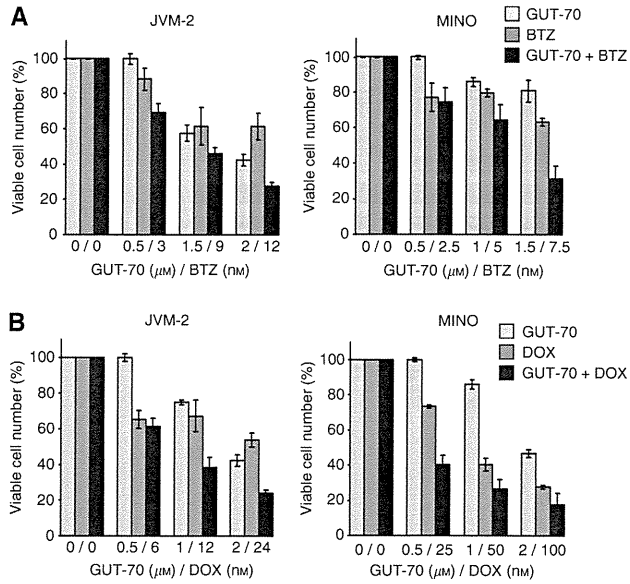

Figure 5 Synergistic interaction between GUT-70 and bortezomib or doxorubicin in MCL cells. JVM2 and MINO cells were cultured in the presence of escalating doses of GUT-70 and bortezomib (BTZ) (**A**) or GUT-70 and doxorubicin (DOX) (**B**) at a fixed ratio. After 48 h, viable and dead cells were identified using the Trypan blue dye exclusion method. Results are expressed as means ± s.d. percentage of viable cell numbers in control cells.

As the client proteins of Hsp90 chaperone molecule become misfolded and ubiquitinated by Hsp90 inhibition, and are then downregulated by proteasomal degradation (Issacs *et al*, 2003; Zhang *et al*, 2004), we next tried to determine whether GUT-70 induces protein ubiquitination followed by proteasomal degradation in wt-*p53*-expressing JVM-2 and mt-*p53*-expressing MINO cells. As expected, GUT-70 treatment elevated the level of protein ubiquitination (Figure 3C); subsequent treatment with proteasome inhibitor bortezomib prevented degradation of c-Raf by GUT-70 (Figure 3D). Taken together, these data indicate the interaction of GUT-70 with Hsp90 and the destabilisation of Hsp90 client proteins by GUT-70.

Effect of GUT-70 on apoptosis-related proteins

To characterise the mechanism of GUT-70-induced cell death in MCL cells, we analysed the expression of apoptosis-related Bcl-2 family proteins, the BH3-only proteins Noxa, Puma, and Bim, and the other Bcl-2 family proteins, Mcl-1 and BAK, in MCL cell lines. Results show that GUT-70 induced substantial accumulation of Noxa but not of Puma (Figure 4A). Mutant-*p53*-bearing MCL cells demonstrated earlier Noxa induction than wt-*p53* cells; peak induction of Noxa was observed after 1 h of GUT-70 treatment in MINO, after 8 h in Jeko-1, and after 24 h in JVM-2 and Granta 519 cells. GUT-70 induced upregulation of *Noxa* mRNA levels in all tested cells (Figure 4B).

After 24 h of GUT-70 treatment, levels of antiapoptotic protein Mcl-1 were increased in JVM-2 and Granta 519 cells, but decreased in Jeko-1 and MINO cells (Figure 4A). It is known that Noxa binds preferentially to Mcl-1 (Warr and Shore, 2008), triggers BAK or Bim release from Mcl-1, and then starts the mitochondrial apoptotic pathway (Willis *et al*, 2005; Hauck *et al*, 2009). Concordantly, we detected coimmunoprecipitation between Noxa and Mcl-1 (Figure 4C) in JVM-2 and Granta 519 cells, both of which showed accumulation of Mcl-1 induced by GUT-70. Although total BAK expression levels remained, consistently independent of GUT-70 treatment (Figure 4A), flow cytometric analysis revealed a pronounced increase of activated BAK in MINO, moderate activation in Jeko-1, and only slight activation in JVM-2 and Granta 519 cells after GUT-70 treatment (Figure 4D), activities that are in inverse relation to Mcl-1 expression levels.

Proapoptotic BH-3-only protein Bim was induced by GUT-70 at 24 h in JVM-2 cells but not in the other cell lines (Figure 4A).

GUT-70 does not induce macroautophagy

Increasing evidence indicates that autophagy is one of the important mechanisms of anticancer reagent-induced cell death (Tsujimoto and Shimizu, 2005). In mammals, three modes of autophagy have been identified: macroautophagy, microautophagy, and chaperone-mediated autophagy (Levine and Klionsky, 2004). To investigate the possibility that GUT-70 promotes macroautophagy, we examined the conversion of light chain 3 (LC3) from LC3-I to LC3-II, a marker of autophagosome formation (Kabeya *et al*, 2000). Whereas LC3-II was moderately induced by a low serum culture condition (5%, 40 h) in wt-*p53*-expressing JVM-2 and Granta 519 cells, there was no change in accumulation of LC3-II following further treatment with GUT-70 (24 h). In mt-*p53*-bearing MINO and Jeko-1 cells, neither serum starvation nor GUT-70 treatment induced LC3-II accumulation (Figure 4A).

To assess the morphological changes induced by GUT-70, U2OS-H2BK-EGFP cells were sequentially photographed after exposure to GUT-70. Cells underwent morphological alterations, including cytoplasmic swelling and vacuolisation after 24 h of GUT-70 exposure (cellular oncosis), and cell death peaked at 36 h (secondary necrosis) (Supplementary Material 1 for Quick-Time movies) (Majno and Joris, 1995; Lemasters *et al*, 1998; Van Cruchten and Van Den Broeck, 2002).

Combination of GUT-70 with bortezomib or doxorubicin has synergistic effects on MCL growth inhibition

To determine whether GUT-70 potentiates the commonly used chemotherapeutic agents, we assessed the effects of combinations of GUT-70 with bortezomib, a selective inhibitor of the 26S proteasome, or doxorubicin, a conventional chemodrug for MCL, on viability of wt-*p53* JVM-2 and mt-*p53* MINO cells. As shown in Figure 5A, both of these combination treatments had observable synergistic effects in both cell types 48 h after exposure. The averaged CI values of GUT-70/bortezomib treatment were 0.59 for JVM2 and 0.73 for MINO; for GUT-70/doxorubicin, 0.37 for JVM2 and 0.35 for MINO, indicating strong and moderate synergism, respectively.

DISCUSSION

The natural product-derived tricyclic coumarin GUT-70 exhibited single-agent antiproliferative and proapoptotic activities against MCL cell lines as a novel Hsp90 inhibitor. GUT-70's dose-dependent inhibition of geldanamycin binding to Hsp90α indicates that GUT-70 has direct binding activity to Hsp90, by which GUT-70 induces conformational change in the Hsp90 molecule and interferes with its binding of geldanamycin. This finding agrees with that of previous studies showing that coumarin antibotic novobiocin binds to the Hsp90 C-terminal ATP binding site and affects the binding of geldanamycin at the Hsp90 N-terminal domain through close interaction between amino and carboxy termini in solution (Csermely *et al*, 1998; Hartson *et al*, 1999; Marcu *et al*, 2000; Donnelly *et al*, 2008). GUT-70 induced depletion of Hsp90 client proteins mt-p53, Raf-1, cyclin D1, and Akt, and increased Hsp70, a marker of Hsp90 inhibition; these findings, along with the ubiquitin-dependent proteasomal degradation of

© 2011 Cancer Research UK

Hsp90 client proteins, suggest that GUT-70 functions as an Hsp90 inhibitor.

It is important that mt-*p53*-expressing MCL cells were more sensitive to GUT-70-induced apoptosis than wt-*p53*-bearing MCL cells. In mt-*p53* cells, prominent GUT-70-induced apoptosis was accompanied by minimal cell cycle arrest, which is consistent with a previous report of G_2/M checkpoint abrogation in p53/p21-impaired cells through downregulation of Chk1 and Wee1 by Hsp90 inhibitor that resulted in premature mitotic entry and mitotic death (Tse *et al*, 2009).

Furthermore, GUT-70 induced the most pronounced apoptosis in MINO cells in which GUT-70 treatment depleted overexpressed mt-p53. mt-p53 is known to confer the additional 'gain of function' as the transcription regulator. Transcriptional activation by mt-p53 has been reported for *MDR1* (Sampath *et al*, 2006), c-*MYC* (Frazier *et al*, 1998), or *GRO1* (Yan and Chen, 2009), resulting in cell proliferation, antiapoptosis, and tumourigenicity (Blandino *et al*, 1999). GUT-70-induced degradation of mt-p53 may successfully repress these oncogenic transcriptional activations.

Another important finding of this study is the prominent *p53*-independent Noxa upregulation by GUT-70. Whereas Noxa had been proposed to be a critical mediator of *p53*-dependent apoptosis (Oda *et al*, 2000), *p53*-independent upregulation of Noxa has been described in MCL and B-cell chronic lymphocytic leukaemia (Pérez-Galán *et al*, 2006; Smit *et al*, 2007). Furthermore, GUT-70 induced Noxa protein accumulation extremely early (1 h) in mt-*p53*-bearing MINO cells, indicating independence from transcriptional gene induction. Recently, Noxa degradation by direct interaction with a spliced isoform of the Kruppel-like tumour suppressor (KLF6-SV1) (Difeo *et al*, 2009), or by posttranscriptional stabilisation/destabilisation of *Bim* mRNA (Matsui *et al*, 2007), has been reported. Our findings indicate the possibility of posttranscriptional Noxa stabilisation by GUT-70, which requires further elucidation.

The preferred binding partner of Noxa is the multidomain antiapoptotic Bcl-2 family member Mcl-1. In response to apoptotic stimuli, Noxa binds to Mcl-1, which ultimately leads to activation of BAK by releasing BAK from the BAK–Mcl-1 complex, and triggers BAK-mediated cell death (Chen *et al*, 2005; Warr and Shore, 2008) (Figure S, Supplementary Material 2 (Kuroda and Kimura, 2007)). The balance between Noxa and Mcl-1 is proposed to determine cell fate as death versus survival (Mei *et al*, 2007). GUT-70-induced BAK activation and sequential apoptosis were associated with Mcl-1 accumulation levels; high levels in less-sensitive wt-*p53* cells and low levels in highly sensitive mt-*p53* cells were consistent with previous reports (Pérez-Galán *et al*, 2006; Mei *et al*, 2007).

Autophagy is known to promote both autophagic cell death and cell survival (Kamitsuji *et al*, 2008). Although GUT-70 did not affect autophagosome formation, Hsp90 clients have been shown to be degraded through chaperone-mediated autophagy (Shen *et al*, 2009). The role of GUT-70 in induction of chaperone-mediated autophagy requires further elucidation.

The observed morphological changes in GUT-70-treated cells (e.g., swelling cytoplasm) indicate cellular oncosis (Van Cruchten and Van Den Broeck, 2002), which shares certain mechanisms and alterations with apoptosis, such as loss of mitochondrial permeability and membrane potential (Lemasters *et al*, 1998).

Furthermore, our results demonstrate that GUT-70 can synergise the cytotoxic effects of the proteasome inhibitor bortezomib and the widely used genotoxic chemotherapeutic agent doxorubicin in MCL cells (Brody and Advani, 2006; Goy *et al*, 2009), regardless of p53 status. Previously, a combination of Hsp90 inhibitor geldanamycin and bortezomib was demonstrated to simultaneously disrupt Hsp90 and proteasome function, promote accumulation of ubiquitinated proteins, and enhance antitumour activity in human breast cancer cells (Mimnaugh *et al*, 2004, 2006). Whereas bortezomib induces longer-term remission (Goy *et al*, 2009), patients ultimately succumb to the poor clinical outcome, and there is a critical need to develop the most effective combination. The synergistic effects of GUT-70 and bortezomib may offer more efficacy and flexibility to the treatment of MCL with bortezomib. The antiproliferative effect of the combination of doxorubicin and GUT-70 was consistent with the previous findings for doxorubicin and Hsp-90 inhibitor 17-(dimethylaminoethylamino)-17-demethoxygeldamanycin (DMAG), which induced premature mitosis, followed by apoptosis, by bypassing the G_2/M checkpoint in lymphoma cells (Robles *et al*, 2006). The synergy with doxorubicin suggests that addition of GUT-70 may allow reduction in the therapeutic dose of doxorubicin, which could potentially reduce its genotoxic side effects (Brody and Advani, 2006). A development of *in vivo* studies of these combination treatments for MCL is further required.

In conclusion, our results demonstrate that the novel anticancer agent GUT-70, a tricyclic coumarin, inhibits cell proliferation by depleting Hsp90 substrates cyclin D1, Akt, and Raf-1, and induces mitochondrial apoptotic cell death with upregulation of Noxa in MCL cells. Notably, these effects are substantially pronounced in MCL cells with mt-*p53*, a known negative prognostic factor for MCL. These findings suggest that GUT-70 has potential utility for the treatment of MCL.

ACKNOWLEDGEMENTS

We thank Drs Kazuhisa Iwabuchi and Akimasa Someya for invaluable help and discussion; Tomomi Ikeda and Takako Shigihara-Ikegami for technical assistance; and Drs Mark Raffeld and Masao Seto for the gifts of cell lines. We thank Katy Hale for manuscript review. This work was supported by the Project Research Program of Juntendo University School of Medicine (to LJ), the Japan Leukemia Research Fund (to YT) and the Research for Promoting Technological Seeds of the Japan Science and Technology Agency (to SK).

Supplementary Information accompanies the paper on British Journal of Cancer website (http://www.nature.com/bjc)

REFERENCES

Bao R, Lai CJ, Qu H, Wang D, Yin L, Zifcak B, Atoyan R, Wang J, Samson M, Forrester J, DellaRocca S, Xu GX, Tao X, Zhai HX, Cai X, Qian C (2009) CUDC-305, a novel synthetic HSP90 inhibitor with unique pharmacologic properties for cancer therapy. *Clin Cancer Res* **15:** 4046–4057

Blandino G, Levine AJ, Oren M (1999) Mutant p53 gain of function: differential effects of different p53 mutants on resistance of cultured cells to chemotherapy. *Oncogene* **18:** 477–485

Bodrug SE, Warner BJ, Bath ML, Lindeman GJ, Harris AW, Adams JM (1994) Cyclin D1 transgene impedes lymphocyte maturation and collaborates in lymphomagenesis with the *myc* gene. *EMBO J* **13:** 2124–2130

Brody J, Advani R (2006) Treatment of mantle cell lymphoma: current approach and future directions. *Crit Rev Oncol Hematol* **58:** 257–265

Chen L, Willis SN, Wei A, Smith BJ, Fletcher JI, Hinds MG, Colman PM, Day CL, Adams JM, Huang DC (2005) Differential targeting of prosurvival Bcl-2 proteins by their BH3-only ligands allows complementary apoptotic function. *Mol Cell* **17:** 393–403

Chou TC, Talalay P (1984) Quantitative analysis of dose-effect relationships: the combined effects of multiple drugs or enzyme inhibitors. *Adv Enzyme Regul* **22:** 27–55

© 2011 Cancer Research UK

Csermely P, Schnaider T, Soti C, Prohaszka Z, Nardai G (1998) The 90-kDa molecular chaperone family: structure, function, and clinical applications. A comprehensive review. *Pharmacol Ther* **79:** 129–168

Difeo A, Huang F, Sangodkar J, Terzo EA, Leake D, Narla G, Martignetti JA (2009) KLF6-SV1 is a novel antiapoptotic protein that targets the BH3-only protein NOXA for degradation and whose inhibition extends survival in an ovarian cancer model. *Cancer Res* **69:** 4733–4741

Döhner H, Fischer K, Bentz M, Hansen K, Benner A, Cabot G, Diehl D, Schlenk R, Coy J, Stilgenbauer S, Volkmann M, Galle PR, Poustka A, Hunstein W, Lichter P (1995) p53 gene deletion predicts for poor survival and non-response to therapy with purine analogs in chronic B-cell leukemias. *Blood* **85:** 1580–1589

Donnelly AC, Mays JR, Burlison JA, Nelson JT, Vielhauer G, Holzbeierlein J, Blagg BS (2008) The design, synthesis, and evaluation of coumarin ring derivatives of the novobiocin scaffold that exhibit antiproliferative activity. *J Org Chem* **73:** 8901–8920

Elo MA, Kaarniranta K, Helminen HJ, Lammi MJ (2005) Hsp90 inhibitor geldanamycin increases hsp70 mRNA stabilisation but fails to activate HSF1 in cells exposed to hydrostatic pressure. *Biochim Biophys Acta* **1743:** 115–119

Fernàndez V, Hartmann E, Ott G, Campo E, Rosenwald A (2005) Pathogenesis of mantle-cell lymphoma: all oncogenic roads lead to dysregulation of cell cycle and DNA damage response pathways. *J Clin Oncol* **23:** 6364–6369

Fløtenes VA, Maelandsmo GM, Forus A, Andreassen A, Myklebost O, Fodstad O (1994) MDM2 gene amplification and transcript levels in human sarcomas: relationship to TP53 gene status. *J Natl Cancer Inst* **86:** 1297–1302

Frazier MW, He X, Wang J, Gu Z, Cleveland JL, Zambetti GP (1998) Activation of c-myc gene expression by tumor-derived p53 mutants requires a discrete C-terminal domain. *Mol Cell Biol* **18:** 3735–3743

Gooljarsingh LT, Fernandes C, Yan K, Zhang H, Grooms M, Johanson K, Sinnamon RH, Kirkpatrick RB, Kerrigan J, Lewis T, Arnone M, King AJ, Lai Z, Copeland RA, Tummino PJ (2006) A biochemical rationale for the anticancer effects of Hsp90 inhibitors: slow, tight binding inhibition by geldanamycin and its analogues. *Proc Natl Acad Sci USA* **103:** 7625–7630

Goy A, Bernstein SH, Kahl BS, Djulbegovic B, Robertson MJ, de Vos S, Epner E, Krishnan A, Leonard JP, Lonial S, Nasta S, O'Connor OA, Shi H, Boral AL, Fisher RI (2009) Bortezomib in patients with relapsed or refractory mantle cell lymphoma: updated time-to-event analyses of the multicenter phase 2 PINNACLE study. *Ann Oncol* **20:** 520–525

Greiner TC, Dasgupta C, Ho VV, Weisenburger DD, Smith LM, Lynch JC, Vose JM, Fu K, Armitage JO, Braziel RM, Campo E, Delabie J, Gascoyne RD, Jaffe ES, Muller-Hermelink HK, Ott G, Rosenwald A, Staudt LM, Im MY, Karaman MW, Pike BL, Chan WC, Hacia JG (2006) Mutation and genomic deletion status of ataxia telangiectasia mutated (*ATM*) and *p53* confer specific gene expression profiles in mantle cell lymphoma. *Proc Natl Acad Sci USA* **103:** 2352–2357

Hartson SD, Thulasiraman V, Huang W, Whitesell L, Matts RL (1999) Molybdate inhibits Hsp90, induces structural changes in its C-terminal domain, and alters its interactions with substrates. *Biochemistry* **38:** 3837–3849

Hauck P, Chao BH, Litz J, Krystal GW (2009) Alterations in the Noxa/Mcl-1 axis determine sensitivity of small cell lung cancer to the BH3 mimetic ABT-737. *Mol Cancer Ther* **8:** 883–892

Issacs JS, Xu W, Neckers L (2003) Heat shock protein 90 as a molecular target for cancer therapeutics. *Cancer Cell* **3:** 213–217

Jadayel DM, Lukas J, Nacheva E, Bartkova J, Stranks G, De Schouwer PJ, Lens D, Bartek J, Dyer MJ, Kruger AR, Catovsky D (1997) Potential role for concurrent abnormalities of the cyclin D1, *p16CDKN2* and *p15CDKN2B* genes in certain B-cell non-Hodgkin's lymphomas: functional studies in a cell line (Granta 519). *Leukemia* **11:** 64–72

Jares P, Colomer D, Campo E (2007) Genetic and molecular pathogenesis of mantle cell lymphoma: perspectives for new targeted therapeutics. *Nat Rev Cancer* **7:** 750–762

Kabeya Y, Mizushima N, Ueno T, Yamamoto A, Kirisako T, Noda T, Kominami E, Ohsumi Y, Yoshimori T (2000) LC3, a mammalian homologue of yeast Apg8p, is localized in autophagosome membranes after processing. *EMBO J* **19:** 5720–5728

Kamitsuji Y, Kuroda J, Kimura S, Toyokuni S, Watanabe K, Ashihara E, Tanaka H, Yui Y, Watanabe M, Matsubara H, Mizushima Y, Hiraumi Y, Kawata E, Yoshikawa T, Maekawa T, Nakahata T, Adachi S (2008) The Bcr-Abl kinase inhibitor INNO-406 induces autophagy and different modes of cell death execution in Bcr-Abl-positive leukemias. *Cell Death Differ* **15:** 1712–1722

Kimura S, Ito C, Jyoko N, Segawa H, Kuroda J, Okada M, Adachi S, Nakahata T, Yuasa T, Filho VC, Furukawa H, Maekawa T (2005) Inhibition of leukemic cell growth by a novel anti-cancer drug (GUT-70) from *Calophyllum brasiliense* that acts by induction of apoptosis. *Int J Cancer* **113:** 158–165

Kuroda J, Kimura S (2007) The role of BH3-only proteins in cancer and anti-cancer therapeutics. *Cell Apoptosis Research Trends*. In Zhang CV (ed) pp 1–39. Nova: New York

Lai R, McDonnell TJ, O'Connor SL, Medeiros LJ, Oudat R, Keating M, Morgan MB, Curiel TJ, Ford RJ (2002) Establishment and characterization of a new mantle cell lymphoma cell line, MINO. *Leuk Res* **26:** 849–855

Lemasters JJ, Nieminen AL, Qian T, Trost LC, Elmore SP, Nishimura Y, Crowe RA, Cascio WE, Bradham CA, Brenner DA, Herman B (1998) The mitochondrial permeability transition in cell death: a common mechanism in necrosis, apoptosis and autophagy. *Biochim Biophys Acta* **1366:** 177–196

Levine B, Klionsky DJ (2004) Development by self-digestion: molecular mechanisms and biological functions of autophagy. *Dev Cell* **6:** 463–477

Majno G, Joris I (1995) Apoptosis, oncosis, and necrosis. An overview of cell death. *Am J Pathol* **146:** 3–15

Marcu MG, Schulte TW, Neckers L (2000) Novobiocin and related coumarins and depletion of heat shock protein 90-dependent signaling proteins. *J Natl Cancer Inst* **92:** 242–248

Matsui H, Asou H, Inaba T (2007) Cytokines direct the regulation of Bim mRNA stability by heat-shock cognate protein 70. *Mol Cell* **25:** 99–112

Mei Y, Xie C, Xie W, Tian X, Li M, Wu M (2007) Noxa/Mcl-1 balance regulates susceptibility of cells to camptothecin-induced apoptosis. *Neoplasia* **9:** 871–881

Melo JV, Brito-Babapulle V, Foroni L, Robinson DS, Luzzatto L, Catovsky D (1986) Two new cell lines from B-prolymphocytic leukaemia: characterization by morphology, immunological markers, karyotype and Ig gene rearrangement. *Int J Cancer* **38:** 531–538

Mimnaugh EG, Xu W, Vos M, Yuan X, Isaacs JS, Bisht KS, Gius D, Neckers L (2004) Simultaneous inhibition of hsp 90 and the proteasome promotes protein ubiquitination, causes endoplasmic reticulum-derived cytosolic vacuolization, and enhances antitumor activity. *Mol Cancer Ther* **3:** 551–566

Mimnaugh EG, Xu W, Vos M, Yuan X, Neckers L (2006) Endoplasmic reticulum vacuolization and valosin-containing protein relocalization result from simultaneous hsp90 inhibition by geldanamycin and proteasome inhibition by velcade. *Mol Cancer Res* **4:** 667–681

Muller P, Hrstka R, Coomber D, Lane DP, Vojtesek B (2008) Chaperone-dependent stabilization and degradation of p53 mutants. *Oncogene* **27:** 3371–3383

Oda E, Ohki R, Murasawa H, Nemoto J, Shibue T, Yamashita T, Tokino T, Taniguchi T, Tanaka N (2000) Noxa, a BH3-only member of the Bcl-2 family and candidate mediator of *p53*-induced apoptosis. *Science* **288:** 1053–1058

Pérez-Galán P, Roué G, Villamor N, Campo E, Colomer D (2006) The proteasome inhibitor bortezomib induces apoptosis in mantle-cell lymphoma through generation of ROS and Noxa activation independent of *p53* status. *Blood* **107:** 257–264

Pratt WB, Toft DO (2003) Regulation of signaling protein function and trafficking by the hsp90/hsp70-based chaperone machinery. *Exp Biol Med* **228:** 111–133

Quintanilla-Martinez L, Davies-Hill T, Fend F, Calzada-Wack J, Sorbara L, Campo E, Jaffe ES, Raffeld M (2003) Sequestration of p27Kip1 protein by cyclin D1 in typical and blastic variants of mantle cell lymphoma (MCL): implications for pathogenesis. *Blood* **101:** 3181–3187

Raynaud SD, Bekri S, Leroux D, Grosgeorge J, Klein B, Bastard C, Gaudray P, Simon MP (1993) Expanded range of 11q13 breakpoints with differing patterns of cyclin D1 expression in B-cell malignancies. *Genes Chromosomes Cancer* **8:** 80–87

Robles AI, Wright MH, Gandhi B, Feis SS, Hanigan CL, Wiestner A, Varticovski L (2006) Schedule-dependent synergy between the heat shock protein 90 inhibitor 17-(dimethylaminoethylamino)-17-demethoxy-geldanamycin and doxorubicin restores apoptosis to p53-mutant lymphoma cell lines. *Clin Cancer Res* **12:** 6547–6556

Sampath J, Sun D, Kidd VJ, Grenet J, Gandhi A, Shapiro LH, Wang Q, Zambetti GP, Schuetz JD (2006) Mutant p53 cooperates with ETS and selectively up-regulates human MDR1 not MRP1. *Clin Cancer Res* **12:** 3459–3469

Samraj AK, Stroh C, Fischer U, Schulze-Osthoff K (2006) The tyrosine kinase Lck is a positive regulator of the mitochondrial apoptosis pathway by controlling Bak expression. *Oncogene* **25:** 186–197

© 2011 Cancer Research UK

Shen S, Zhang P, Lovchik MA, Li Y, Tang L, Chen Z, Zeng R, Ma D, Yuan J, Yu Q (2009) Cyclodepsipeptide toxin promotes the degradation of Hsp90 client proteins through chaperone-mediated autophagy. *J Cell Biol* **185:** 629–639

Sherr CJ, Roberts JM (1999) CDK inhibitors: positive and negative regulators of G_1-phase progression. *Genes Dev* **13:** 1501–1512

Smit LA, Hallaert DY, Spijker R, de Goeij B, Jaspers A, Kater AP, van Oers MH, van Noesel CJ, Eldering E (2007) Differential Noxa/Mcl-1 balance in peripheral versus lymph node chronic lymphocytic leukemia cells correlates with survival capacity. *Blood* **109:** 1660–1668

Tse AN, Sheikh TN, Alan H, Chou TC, Schwartz GK (2009) 90-kDa heat shock protein inhibition abrogates the topoisomerase I poison-induced G2/M checkpoint in p53-null tumor cells by depleting Chk1 and Wee1. *Mol Pharmacol* **75:** 124–133

Tsujimoto Y, Shimizu S (2005) Another way to die: autophagic programmed cell death. *Cell Death Differ* **12:** 1528–1534

Van Cruchten S, Van Den Broeck W (2002) Morphological and biochemical aspects of apoptosis, oncosis and necrosis. *Anat Histol Embryol* **31:** 214–223

Warr MR, Shore GC (2008) Unique biology of Mcl-1: therapeutic opportunities in cancer. *Curr Mol Med* **8:** 138–147

Willis SN, Chen L, Dewson G, Wei A, Naik E, Fletcher JI, Adams JM, Huang DC (2005) Proapoptotic Bak is sequestered by Mcl-1 and Bcl-xL, but not Bcl-2, until displaced by BH3-only proteins. *Genes Dev* **19:** 1294–1305

Yan W, Chen X (2009) Identification of GRO1 as a critical determinant for mutant p53 gain of function. *J Biol Chem* **284:** 12178–12187

Zhang R, Luo D, Miao R, Bai L, Ge Q, Sessa WC, Min W (2005) Hsp90-Akt phosphorylates ASK1 and inhibits ASK1-mediated apoptosis. *Oncogene* **24:** 3954–3963

Zhang Y, Wang JS, Chen LL, Cheng XK, Heng FY, Wu NH, Shen YF (2004) Repression of hsp90beta gene by p53 in UV irradiation-induced apoptosis of Jurkat cells. *J Biol Chem* **279:** 42545–42551

© 2011 Cancer Research UK

Supplemental Material can be found at:
http://www.jbc.org/content/suppl/2010/12/16/M110.167742.DC1.html

THE JOURNAL OF BIOLOGICAL CHEMISTRY VOL. 286, NO. 7, pp. 5589–5598, February 18, 2011
© 2011 by The American Society for Biochemistry and Molecular Biology, Inc. Printed in the U.S.A.

The Dynactin Complex Maintains the Integrity of Metaphasic Centrosomes to Ensure Transition to Anaphase*[S]

Received for publication, July 22, 2010, and in revised form, December 14, 2010 Published, JBC Papers in Press, December 16, 2010, DOI 10.1074/jbc.M110.167742

Yuko Ozaki, Hirotaka Matsui, Akiko Nagamachi, Hiroya Asou, Daisuke Aki, and Toshiya Inaba[1]

From the Department of Molecular Oncology and Leukemia Program Project, Research Institute for Radiation Biology and Medicine, Hiroshima University, Hiroshima 734-8553, Japan

The dynactin complex is required for activation of the dynein motor complex, which plays a critical role in various cell functions including mitosis. During metaphase, the dynein-dynactin complex removes spindle checkpoint proteins from kinetochores to facilitate the transition to anaphase. Three components ($p150^{Glued}$, dynamitin, and p24) compose a key portion of the dynactin complex, termed the projecting arm. To investigate the roles of the dynactin complex in mitosis, we used RNA interference to down-regulate p24 and $p150^{Glued}$ in human cells. In response to p24 down-regulation, we observed cells with delayed metaphase in which chromosomes frequently align abnormally to resemble a "figure eight," resulting in cell death. We attribute the figure eight chromosome alignment to impaired metaphasic centrosomes that lack spindle tension. Like p24, RNA interference of $p150^{Glued}$ also induces prometaphase and metaphase delays; however, most of these cells eventually enter anaphase and complete mitosis. Our findings suggest that although both p24 and $p150^{Glued}$ components of the dynactin complex contribute to mitotic progression, p24 also appears to play a role in metaphase centrosome integrity, helping to ensure the transition to anaphase.

The dynein-dynactin complex, a minus end-directed microtubule-based motor, carries out diverse transport activities indispensable for various cell functions and behaviors (Ref. 1 and references therein). For instance, the dynein-dynactin complex transports giant centrosomal scaffold proteins such as CG-NAP/AKAP450 and NuMA and induces smooth progression through mitosis. This motor complex also contributes to the transition from metaphase to anaphase: To ensure that each daughter cell receives only one chromosome set, the spindle assembly checkpoint blocks entry into anaphase until kinetochores on sister chromatids are attached to opposite spindle poles. Once this condition is achieved, the dynein-dynactin motor induces passage through the spindle checkpoint by removing critical checkpoint proteins (such as BubR1 or Mad2) from kinetochores.

* This work was supported by grants-in-aid for scientific research from the Ministry of Education, Culture, Sports, Science and Technology of Japan.
[S] The on-line version of this article (available at http://www.jbc.org) contains supplemental Movies 1–3.
[1] To whom correspondence should be addressed: 1-2-3 Kasumi, Minami-ku, Hiroshima 734-8553, Japan. Fax: 81-82-256-7103; E-mail: tinaba@hiroshima-u.ac.jp.

Dynactin is composed of 10 subunit proteins that are required for dynein activation (2) and references therein). Three proteins among them, $p150^{Glued}$ (dynactin 1), dynamitin (p50 and dynactin 2), and p24 (dynactin 3) (3, 4), constitute a flexible and extendable structure (the projecting arm) that associates directly with microtubules and the dynein complex.

Each dynactin molecule contains two copies of $p150^{Glued}$ and p24 and four copies of dynamitin. All three proteins are evolutionarily conserved from yeast to mammalian cells (5, 6), suggesting that these components are essential for the formation of a functional projecting arm. Within this substructure, $p150^{Glued}$ is sufficient for binding to dynein and for traversing the microtubule lattice, whereas dynamitin also plays a critical role in association with the dynein complex and in promotion of dynein-based movement. It is noteworthy that overexpression of dynamitin disrupts dynactin structure (7). Although the mechanism underlying this disruption is yet to be elucidated, dynamitin overexpression has been the major tool in molecular biology for down-regulation of dynactin function (2). Indeed, dynamitin overexpression was used to verify involvement of the dynactin complex in the spindle checkpoint silencing that induces metaphase arrest/delay (8).

In contrast to $p150^{Glued}$ or dynamitin, little is known about the role of the p24 subunit in mitosis. Although Ldb18 (a *Saccharomyces cerevisiae* homolog of p24) is essential for attachment of $p150^{Glued}$ to dynamitin and to the remainder of the dynactin complex (6), low amino acid identity between Ldb18 and human p24 (16.9%) does not favor speculation on the roles of mammalian p24.

RNAi is currently the most useful method for down-regulating the expression of a specific gene. Although several authors report successful suppression of $p150^{Glued}$ using siRNA or shRNA (8–10), their papers did not describe any mitotic abnormalities in cells expressing reduced levels of $p150^{Glued}$. Moreover, there have been no reports of p24 down-regulation using the RNAi method. In this report, we use RNAi to down-regulate p24 and $p150^{Glued}$ proteins in human cells. Our results demonstrate that cells expressing reduced levels of either p24 or $p150^{Glued}$ both show severe metaphase delay but that other mitotic disturbances differ between the two suppressed genes.

EXPERIMENTAL PROCEDURES

Cell Culture and Transfection of siRNA—HeLa, U2OS, and HEK 293 cell lines and their derivative cells were cultured in Dulbecco's modified Eagle's medium supplemented with 10% FBS. siRNA oligonucleotides for $p150^{Glued}$ (siRNA-p150, 5′-

Downloaded from www.jbc.org at HIROSHIMA UNIVERSITY, on February 15, 2011

GACTTCACCCCTTGATTAA-3′; siRNA-p150b, 5′-CCACCACCAAAGGUUAAGU-3′) (10) or p24 (siRNA-p24, 5′-CCGCATTGCCATACCTGAT-3; siRNA-p24b, 5′-GCUACUUUGCCAGCUAGAG-3′) were transfected at a concentration of 100 nM into HeLa(tc), a HeLa subline (11) or U2OS cells using Oligofectamine (Invitrogen), otherwise indicated in text and figure legends. Dead cells were identified using the trypan blue dye exclusion test. p24 and H2B-GFP were expressed using the pcDNA3 expression vector (Invitrogen).

Rescue Experiments—An siRNA-p24-resistant p24 cDNA was created by changing six nucleotides in the target sequence of siRNA-p24 that have no effect on amino acid sequence (CCGAATAGCAATCCCAGAC; underlined letters indicate replaced nucleotides). Because the target sequence for siRNA-p150 is in the 3′-UTR, we used a p150 cDNA 3′-UTR truncation (a gift of Dr. M. Katsuno and G. Sobue (12)) to generate a siRNA-p150-resistant p150 cDNA. To generate a pantropic retrovirus, HEK 293 cells were co-transfected with three plasmids: pHIT60 expressing murine leukemia virus gag pol (a gift of Dr. A. J. Kingsman (13)), pHCMV-G for vesicular stomatitis virus enveloped pseudotypes (a gift of Dr. T. Friedmann (14)), and pMSCV (Clontech) driving expression of siRNA-resistant p24 or p150 cDNA and IRES-EGFP[2] (15).

Analysis of mRNA and Protein Expression—Real-time quantitative RT-PCR was performed as described previously (16) using primer sets (p24 (forward, 5′-GAGTACATCGACCGCATTGCCATAC-3′ and reverse, 5′-TGATGTGAGCACTGTCCAGCATGG-3′) and $p150^{Glued}$ (forward, 5′-TGCAGGCCACGCTACACCGCTATG-3′ and reverse, 5′-GCAATATCTGTAGCCTCCTGCCCAC-3′)). Immunostaining and image analyses were performed as described (11, 17). Signal specificity was tested by adding antigen for each antibody into the blocking solution. Relative fluorescence intensity was measured using ImageJ software. Immunoprecipitation and immunoblot analyses were performed according to standard procedures (18).

TUNEL—TUNEL assays were performed using the Fluorometric TUNEL assay kit (Promega, Madison, WI). Briefly, cells fixed with paraformaldehyde and ethanol were incubated with fluorescein-dUTP and terminal deoxynucleotidyl transferase for one hour at 37 °C. Cells were propidium iodide-stained immediately prior to flow cytometry analysis (FACSCalibur, BD Biosciences).

Fluorescence in Situ Hybridization (FISH)—HeLa cells cultured on coverglass slips were fixed with 3.7% formaldehyde, denatured on a heat block, and used directly for FISH analysis using a Myc probe complementary to chromosome band 8q24 (Dako, Glostrup, Denmark) according to the manufacturer's protocol.

Reagents—Rabbit anti-p24 polyclonal antibodies were raised against a GST-p24(N) (amino acids 5–36) or a GST-p24(C) polypeptide (amino acids 145–186) and then affinity purified according to standard procedures (18). Commercial antibodies were purchased from the following suppliers: $p150^{Glued}$ from BD Biosciences; actin (product no. 1378 996) from Roche Diagnostics; and α-tubulin (product no. T9026) and γ-tubulin (product no. T6557) from Sigma. Hoechst 33342 was purchased from Invitrogen.

[2] The abbreviations used are: EGFP, enhanced GFP; FISH, fluorescence in situ hybridization; IRES, internal ribosomal entry site.

RESULTS

Down-regulation of p24 and $p150^{Glued}$ Using siRNA—We initially used HeLa(tc) cells, a HeLa subline that allows high efficiency siRNA transfection (typically >90%) (11), for siRNA transfections. HeLa(tc) cells treated with siRNA (100 nM for 24 h) specific for p24 (siRNA-p24) or $p150^{Glued}$ (siRNA-p150) showed a 5-fold approximate decrease in mRNA expression levels relative to cells treated with scrambled control siRNA (control siRNA) (Fig. 1*A*).

We used rabbits to generate two polyclonal antibodies, p24(N) and p24(C), against different portions of p24 (see "Experimental Procedures"). Both antibodies recognized an endogenous p24 protein (Fig. 1*B*, *lane 1*) that migrated to the same position in SDS-polyacrylamide gels as exogenous p24 protein expressed from a eukaryote plasmid expression vector (*lane 4*). As previously reported, the apparent mass of p24 is ~21 kDa, slightly smaller than the mass predicted from the amino acid sequence (4). Cells treated with siRNA-p24 (100 nM) for 48 h expressed 10-fold lower levels of p24 protein relative to untreated cells or cells treated with control siRNA (*lane 3*). Immunoblot analysis using $p150^{Glued}$ antibody revealed a 20-fold reduction in $p150^{Glued}$ protein levels in cells treated with siRNA-p150 for 72 h (Fig. 1*C*).

Similar to previous reports (4), immunostaining of mitotic cells with p24(C) antibody showed p24 localized to kinetochores and centrosomes in prometaphase and metaphase cells with considerable signal remaining in early anaphase (Fig. 1*D*). Although the general localization of $p150^{Glued}$ (Fig. 1*E*) overlaps with p24, some specific differences were distinguished in cells doubly stained with p24 and $p150^{Glued}$ antibodies (Fig. 1*F*). First, staining of mitotic spindles with anti-p150 was strong, whereas only weak fluorescence was detected with anti-p24. Second, although both p24 and p150 signals were detected at prometaphase kinetochores, p150 signal intensity diminished rapidly in metaphase, whereas p24 signals were remained until anaphase. The contrast between the intense p24 immunofluorescence maintained in anaphase centrosomes with diminished $p150^{Glued}$ immunofluorescence that is barely detectable in early anaphase suggests a rapid efflux of $p150^{Glued}$ from centrosomes during metaphase.

When cells were transfected with Cy3-labeled siRNA-p24, the intensity of p24 immunofluorescence in Cy3 staining-positive cells was reduced (Fig. 1*G*, *left panels*). $p150^{Glued}$ signals were also reduced in response to treatment with siRNA-p150 (100 nM) for 72 h (*right panels*).

siRNA-p24 or -p150 Induces Mitotic Disturbances—Although we observed no obvious morphological differences in phase-contrast microscopy images of interphasic HeLa(tc) cells treated for up to 72 h with control siRNA, siRNA-p24, or siRNA-p150 (100 nM) (data not shown), we did observe a significant increase in the mitotic index of cells 48 h after transfection with siRNA-p24 relative to control siRNA (11.1% relative to 4%) ($p < 0.01$, Chi-square test, Fig. 2*A*). In addition,

Downloaded from www.jbc.org at HIROSHIMA UNIVERSITY, on February 15, 2011

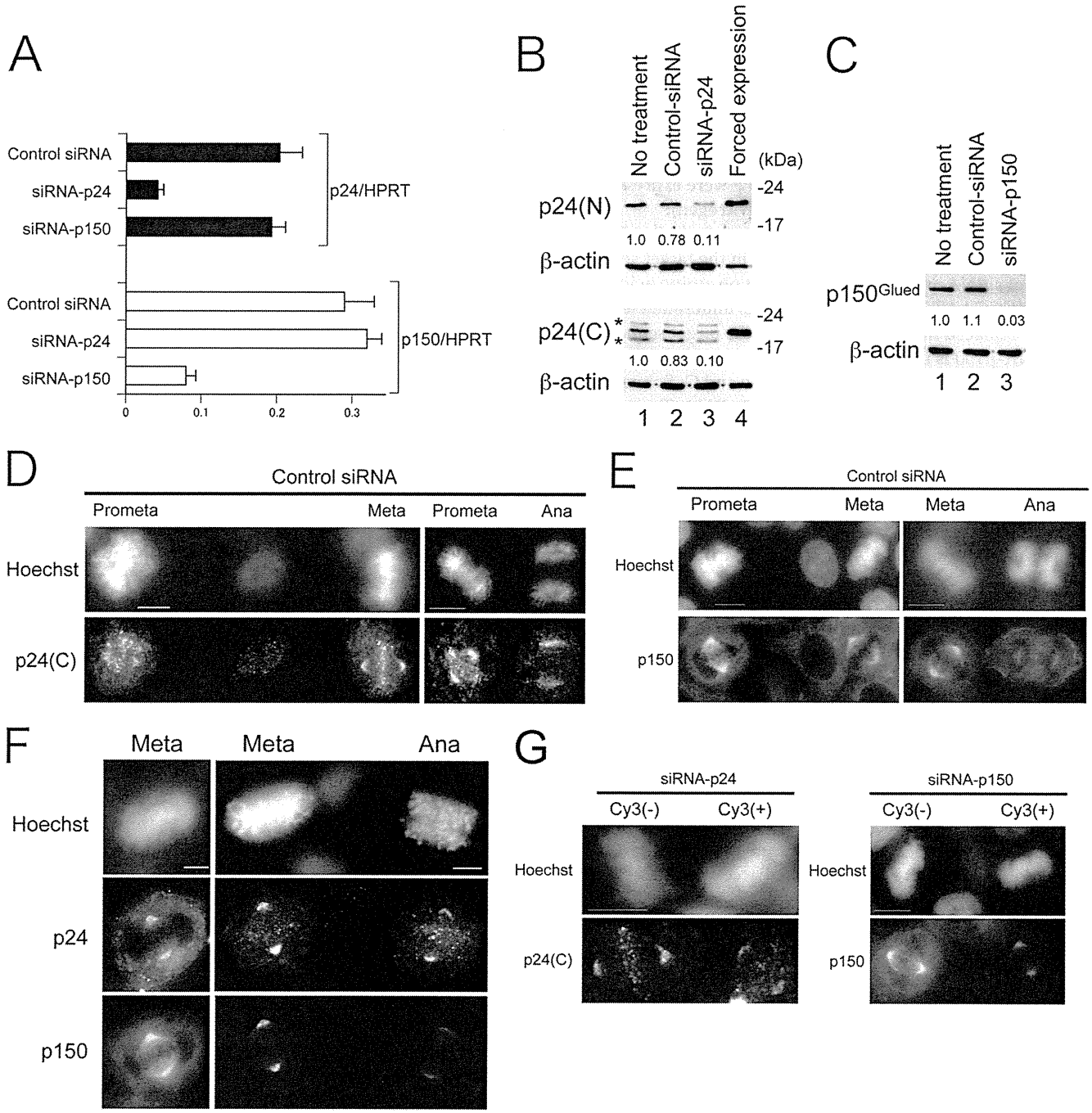

FIGURE 1. **Down-regulation of p24 and p150 by siRNA.** *A*, p24 (*black bars*) and p150^{Glued} (*open bars*) mRNA expression levels in HeLa(tc) cells treated with control siRNA, siRNA-p24, or siRNA-p150 (100 nM) for 24 h. Real-time quantitative PCR data were normalized against hypoxanthine phosphoribosyl transferase (*HPRT*), and the mean and S.D. for three independent experiments is represented. *B*, immunoblot analysis using p24(N), p24(C), or β-actin antibody. *Lane 1*, untreated HeLa(tc) cells; *lane 2*, cells treated with control siRNA (100 nM) for 48 h; *lane 3*, cells treated with siRNA-p24 (100 nM) for 48 h; *lane 4*, HEK 293 cells transfected with pcDNA3-p24, a eukaryotic expression vector. Ratios of relative intensity (p24/actin) measured by densitometry are indicated below each lane. *Asterisks* indicate cross-reactive bands appearing in HeLa but not HEK 293 cells. *C*, immunoblot analysis using p150^{Glued} or β-actin antibody. *Lane 1*, untreated HeLa(tc) cells; *lane 2*, cells treated with control siRNA (100 nM) for 72 h; *lane 3*, cells treated with siRNA-p150 (100 nM) for 72 h. Ratios of relative intensity (p150/actin) measured by densitometry are shown below. *D–G*, immunostaining of mitotic HeLa cells treated with siRNA indicated *above* with antibodies indicated on the *left*. DNA was stained with Hoechst 33342, and the mitotic phase of cells are labeled above. *Bars*, 10 μm (*D*, *E*, and *G*) and 5 μm (*F*). *Meta*, metaphase; *Ana*, anaphase; *Prometa*, prometaphase.

there was also a significant increase ($p < 0.01$) in the number of dead cells (determined by trypan blue dye exclusion) among the cells treated with siRNA-p24 for 48 and 72 h (7.2%, 15/207 and 17.1% 36/211, respectively) and siRNA-p150 for 72 h (8.0%, 16/202) relative to untreated cells (2.0%, 8/401).

Flow cytometric analyses of HeLa cells treated with siRNA-p24 for 48 h and stained with propidium iodide dem-

Downloaded from www.jbc.org at HIROSHIMA UNIVERSITY, on February 15, 2011

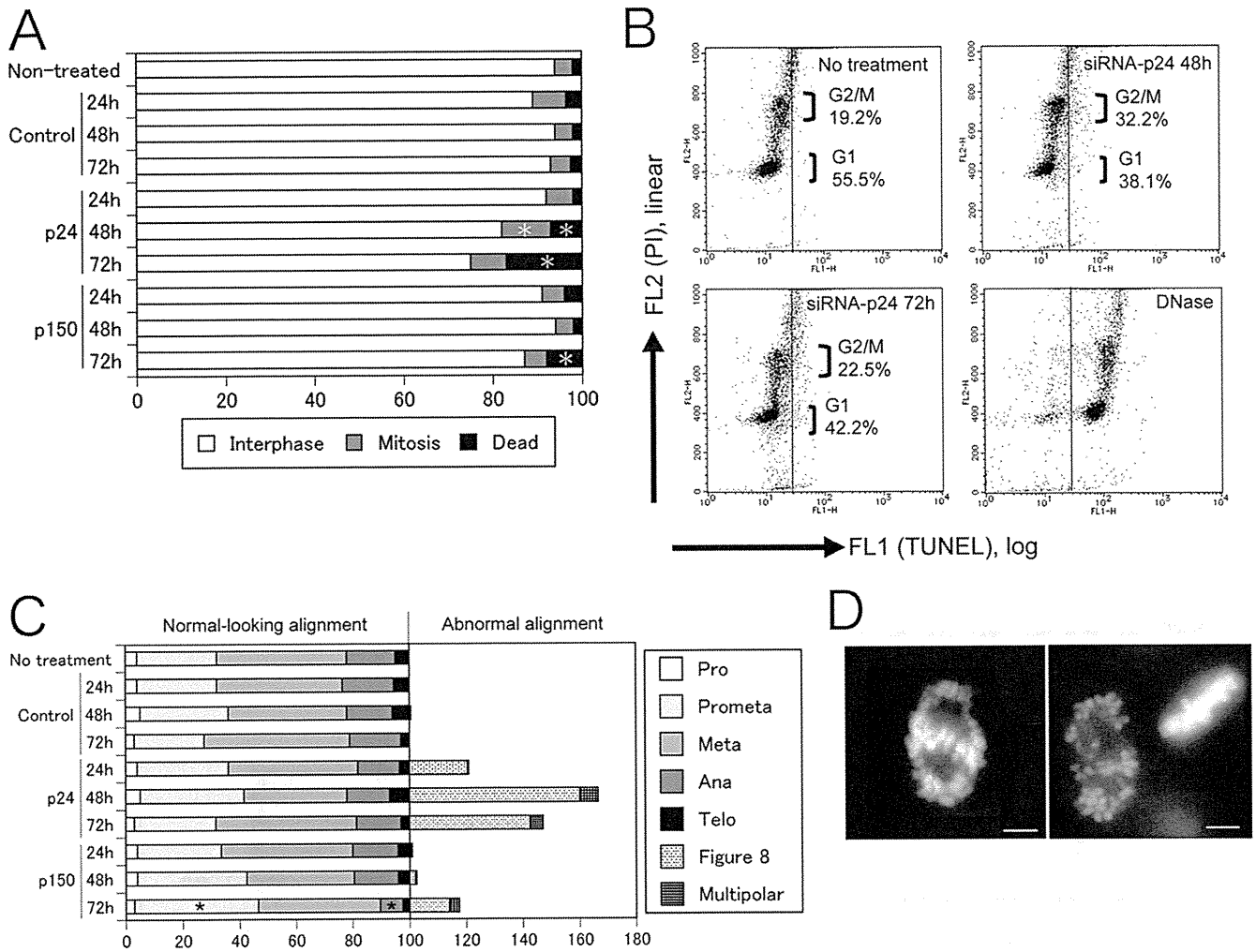

FIGURE 2. **Down-regulation of p24 and p150 induces mitotic abnormalities in HeLa(tc) cells.** *A*, cells were treated with each siRNA for periods indicated on the *left*. From a total of 300 cells counted/treatment, the relative percentages of mitotic, interphase, and dead cells determined by separation of floating cells (mitotic and dead *versus* interphase) and by trypan blue dye exclusion (live *versus* dead) are indicated by *shading*. *Asterisks* indicate a statistically significant ($p < 0.01$) increase relative to the no treatment control using Chi-square test. *B*, cells treated with siRNA-p24 for indicated periods were stained with propidium iodide (*PI*) just prior to flow cytometry and TUNEL analysis. FL1 values on the *horizontal axis* indicate the amount of dUTP polymerized by DNA free 3′ ends, whereas FL2 values on the *vertical axis* show the DNA content. *C*, from a total of 300 cells counted/treatment, the percentages of mitotic cells with normal-looking chromosome alignment (100% total) or abnormal mitosis were determined from observations of Hoechst 33342-stained nuclei. *Asterisks* indicate statistically significant changes in a particular mitotic phase ($p < 0.01$) relative to the no treatment control by Chi-square test. *D*, representative images of Hoescht 33342-stained chromosomes in a figure eight alignment. *Bar*, 5 μm. *Pro*, prophase; *Prometa*, prometaphase; *Meta*, metaphase; *Ana*, anaphase; *Telo*, telophase.

onstrate that siRNA-p24 induces mitotic delay/arrest, in that the G_2/M-phase ratio (Fig. 2*B*, *vertical axis*) was significantly higher in treated cells (32.2%) than in cells without treatment (19.2%) However, the cell death induced by siRNA-p24 does not appear apoptotic because TUNEL assays showed only a small increase in DNA free 3′ ends (Fig. 2*B*, *horizontal axis*; see DNase-treated HeLa cell panel as a positive control) in siRNA-p24-treated cells.

To determine the effects of down-regulation of p24 and $p150^{Glued}$ on mitosis, we analyzed chromosome alignment in Hoechst 33342-stained mitotic cells. Although treatment of cells with control siRNA (100 nM) for up to 72 h did not affect their distribution (Fig. 2*C*), we observed that treatment with siRNA-p24 for 48 h specifically induced one of two distinct patterns of abnormal chromosome alignment in 39.8% (133/334) of mitotic cells (Fig. 2*C*). First, chromosomes in 120 mitotic cells treated with siRNA-p24 for 48 h aligned abnormally to resemble a figure eight pattern (Fig. 2*D*), whereas the same pattern almost never appeared (<1/200) in mitotic cells without siRNA treatment or those treated with control siRNA. Second, 3.9% (13/334) of mitotic cells treated with siRNA-p24 for 48 h demonstrated multipolar mitoses. Among the remaining 201 mitotic cells with normal-looking chromosome alignment, the distribution of cells in each mitotic phase was not altered. Relative to cells treated for 48 h, cells treated with siRNA-p24 for 24 or 72 h showed the same abnormal pattern of chromosome alignment but at a lower frequency (Fig. 2*C*).

In contrast to siRNA-p24-treated cells, cells treated with siRNA-p150 for 48 h showed no significant change in distribution among mitotic phases, and only a few cells demon-

Downloaded from www.jbc.org at HIROSHIMA UNIVERSITY, on February 15, 2011

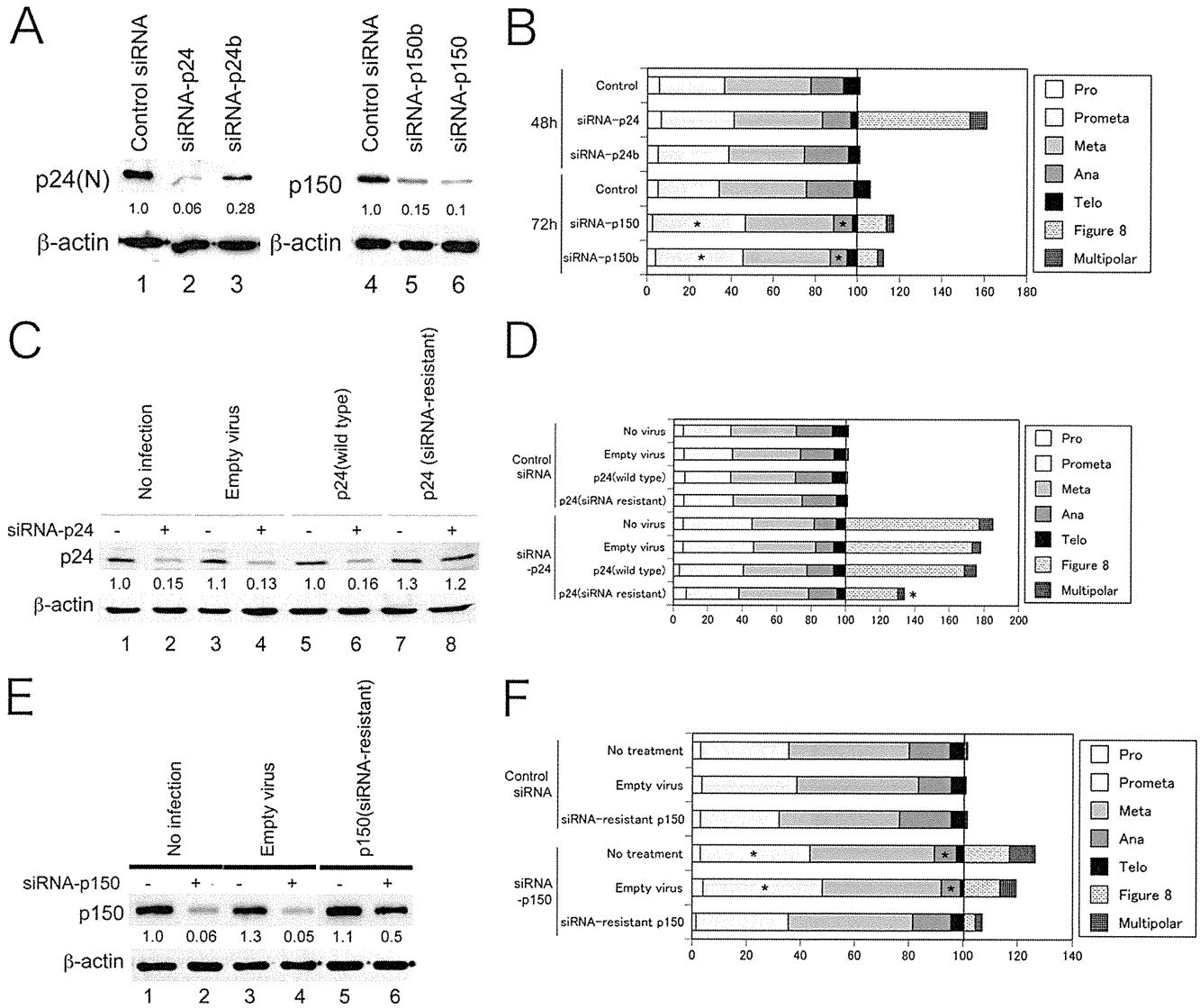

FIGURE 3. *A*, immunoblot analysis using p24(N), p150, or β-actin antibody. HeLa(tc) cells were treated with the siRNA (100 nM) indicated above for 48 (*lanes 1–3*) or 72 h (*lanes 4–6*). Ratios of signal intensity relative to actin (measured using densitometry) are indicated *below each lane*. *B*, *D*, and *F*, the percentages of mitotic cells with normal-looking chromosome alignment (100% total) or abnormal mitosis were determined from observations of Hoechst 33342-stained nuclei in a total of 300 cells/treatment. *Asterisks* indicate statistically significant changes in a particular mitotic phase ($p < 0.01$) relative to the no treatment control using the Chi-square test. *C*, immunoblot analyses using p24(N) or β-actin antibody. *Lanes 1* and *2*, uninfected HeLa(tc) cells; *lanes 3* and *4*, cells infected with empty virus; *lanes 5* and *6*, cells infected with virus containing wild type p24 cDNA; *lanes 7* and *8*, cells infected with virus containing siRNA-resistant p24 cDNA. *Lanes 1*, *3*, *5*, and *7*, cells were treated with control siRNA; *lanes 2*, *4*, *6*, and *8*, cells were treated with siRNA-p24 (100 nM) for 48 h. Ratios of relative signal intensity (p24/actin) are indicated *below each lane*. *E*, immunoblot analysis using p150 or β-actin antibody. *Lanes 1* and *2*, uninfected HeLa(tc) cells; *lanes 3* and *4*, cells infected with empty virus; *lanes 5* and *6*, cells infected with virus containing siRNA-resistant p150 cDNA. *Lanes 1*, *3*, and *5*, cells were treated with control siRNA; *lanes 2*, *4*, and *6*, cells were treated with siRNA-p150 (100 nM) for 72 h. Ratios of relative intensity (p150/actin) are indicated *below each lane*. *Pro*, prophase; *Prometa*, prometaphase; *Meta*, metaphase; *Ana*, anaphase; *Telo*, telophase.

strated the figure eight chromosome alignment seen with siRNA-p24 (Fig. 2*C*). After an additional 24 h of treatment with siRNA-p150, however, we observed a significant increase in the ratio of prometaphase cells and a corresponding decrease in anaphase and telophase cells. In addition, small percentages of mitotic cells showed the figure eight chromosomal alignment (11.9%, 28/236) or multipolar mitoses (3.0%, 7/236).

We also treated cells with secondary siRNAs that target alternative sequences in the p24 or p150^{Glued} genes. When cells were treated with siRNA-p24b, which only reduced p24 levels ~3-fold (Fig. 3*A*), few mitotic cells showed the figure eight chromosome alignment (Fig. 3*B*), suggesting that greater reductions in p24 protein levels are required to induce the figure eight alignment. In contrast, cells treated with siRNA-p150b reduced p150 to levels similar to siRNA-p150 (Fig. 3*A*) and showed similar mitotic disturbances, including an increased ratio of prometaphase cells, a decreased ratio of anaphase/telophase cells, and a few cells with figure eight chromosome alignment.

To exclude the possibility that the figure eight chromosome alignment is an off-target effect of siRNA-p24, we performed

Downloaded from www.jbc.org at HIROSHIMA UNIVERSITY, on February 15, 2011

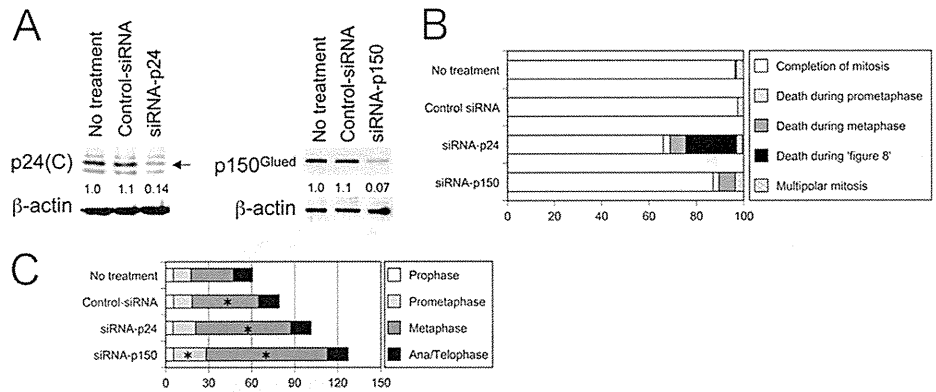

FIGURE 4. **Time-lapse observations of mitotic cells.** *A*, immunoblot analyses of lysates from U2OS cells using p24(C), p150^{Glued}, or β-actin antibody. Cells were treated with the siRNA indicated for 72 h. Ratios of relative intensity (p24 or p150/actin) measured by densitometry are indicated *below each lane*. An *arrow* marks the position of p24. *B*, U2OS cells expressing an H2B-GFP fusion protein were treated with control siRNA or siRNA-p150 for >48 h or with siRNA-p24 for >24 h. Percentages of cells demonstrating termination of mitosis in one of the manners listed on the *right* are indicated with *shading*. *C*, the average duration of each mitotic phase (min) in cells that completed mitosis are indicated by shading. *Asterisks* indicate a statistically significant increase in duration ($p < 0.05$) relative to the no treatment control.

rescue experiments by expressing a siRNA-p24-resistant p24 mRNA from a pantropic retrovirus containing EGFP as a selection marker (see "Experimental Procedures"). EGFP-positive cells were sorted using flow cytometry and then treated with siRNA-p24.

Immunoblot analyses revealed similar levels of p24 in cells infected with retrovirus containing p24 cDNA or siRNA-resistant p24 cDNA (Fig. 3*C*, *lanes 5* and *7*). Following treatment with siRNA-p24 (100 nM for 48 h), uninfected cells, as well as those infected with empty virus or virus containing wild-type cDNA (Fig. 3*C*, *lanes 2*, *4*, and *6*) showed down-regulation of p24 protein. In contrast, there was no significant reduction in p24 levels in cells expressing the siRNA-resistant p24 cDNA (Fig. 3*C*, *lane 8*). Mitotic cells with the figure eight chromosome alignment were observed in cells infected with empty virus (73%) or virus containing wild type cDNA (68.5%) at virtually the same frequency as uninfected cells (77.3%) (Fig. 3*D*). Only cells infected with virus containing the siRNA-resistant cDNA showed a significant reduction in the frequency figure eight mitoses (34.5%, $p < 0.01$), suggesting that p24 is indeed effective in preventing chromosomes from the figure eight alignment.

We also expressed a siRNA-resistant p150 cDNA in HeLa cells using the same pantropic retrovirus system (Fig. 3*E*). Unlike uninfected cells or those infected with the empty virus, cells expressing siRNA-resistant cDNA showed little decrease in p150 levels following siRNA treatment. Similarly, there was no significant increase in prometaphase or decrease in ana/telophase ratios in cells treated with siRNA-p150 (Fig. 3*F*), and the ratio of cells with the figure eight chromosome alignment decreased.

Chromosomes Align into a Figure Eight after Metaphase Arrest—To further analyze the mitotic disturbances induced by p24 or p150^{Glued} down-regulation, we established a U2OS cell line expressing a histone H2B-GFP fusion protein constitutively (19), transfected these cells with control, p24, or p150^{Glued} siRNAs (efficiency typically 70%) and then collected time-lapse images of the transfected cells. In these cells, the magnitude in reduction of p24 or p150^{Glued} protein expression levels by siRNA-p24 or siRNA-p150, respectively, were similar to those achieved in HeLa cells (Fig. 4*A*).

More than 95% of mitotic cells without siRNA treatment or treated with control siRNA completed mitosis (Fig. 4*B*, also see supplemental Movie 1). Cells treated with control siRNA demonstrated a significant elongation of metaphase (46 min in control siRNA-treated cells to compare with 29 min in untreated cells, $p < 0.05$), whereas the durations of prophase, prometaphase, and anaphase and telophase combined (ana/telophase) were not affected (Fig. 4*C*). These data suggest that U2OS cells treated with scrambled siRNA and/or cationic liposome experience a delayed progression through metaphase. Only one of 180 (0.55%) untreated cells and zero of 156 cells treated with control siRNA died while in mitosis.

When cells were treated with siRNA-p24 (100 nM) for >24 h, we observed a significant delay in metaphase (average of 66 min) relative to control siRNA-treated cells (average of 46 min, $p < 0.05$, Fig. 4*C*). There was no elongation in the duration of prometaphase or ana/telophase. We also observed cell death more frequently in siRNA-p24-treated cells: 3% (10/333) or 6.5% (22/333) of mitotic cells underwent cell death during prometaphase or metaphase, respectively (Fig. 4*B*). Intriguingly, in 21.5% (72/333) of siRNA-p24-treated mitotic cells, chromosomes aligned at the metaphase plate during prolonged metaphase broke up into a figure eight pattern (supplemental Movie 2). This similarity to the abnormal chromosome alignment observed in siRNA-p24-treated HeLa cells (Fig. 2*D*) indicates that these are not prometaphase cells but rather post-metaphasic cells that fail to enter anaphase. All 72 cells with figure eight chromosome alignment underwent cell death eventually (an average of 164 min after breakup of chromosome alignment at the metaphase plate) (supplemental Movie 2). Overall, 31% (104/333) of siRNA-p24-treated mitotic cells underwent cell death, whereas these cells in interphase rarely underwent apoptosis (< 0.1%).

In contrast to control siRNA- or siRNA-p24-treated cells, cells treated with siRNA-p150 for >48 h demonstrated delayed prometaphase (average of 23 min to compare with 12 min in control siRNA-treated cells, $p < 0.05$, Fig. 4*C*), during

Downloaded from www.jbc.org at HIROSHIMA UNIVERSITY, on February 15, 2011

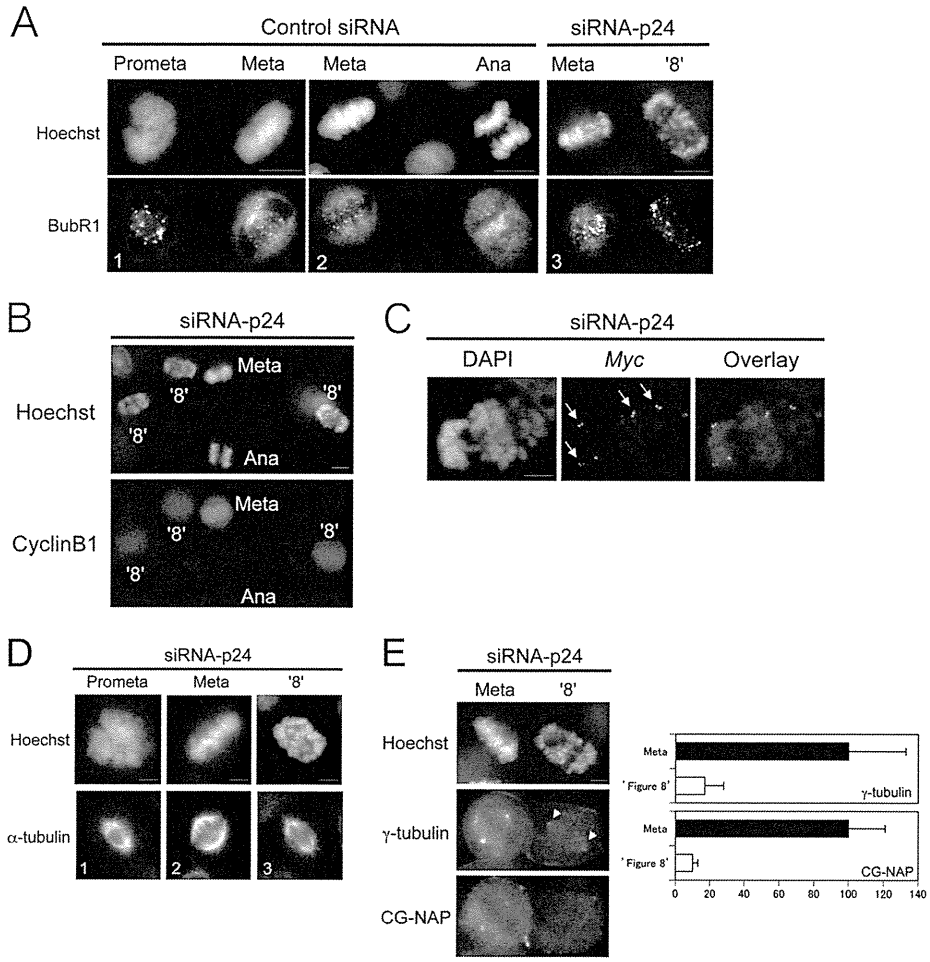

FIGURE 5. **Mechanisms of figure eight chromosome alignment.** *A*, *B*, and *D*, HeLa cells were treated with the siRNA indicated and immunostained with the antibody indicated on the *left*. DNA was stained with Hoechst 33342, and the mitotic phase of cells are labeled *above or within* each image. *Bars*, 10 μm (*A* and *B*) and 5 μm (*D*). *C*, HeLa cells treated with siRNA-p24 were fixed with formaldehyde, denatured, and hybridized with a c-*myc* probe for FISH analysis. DNA was stained with DAPI. *Arrows* mark pairs of dots that indicate sister chromatids. *Bar*, 5 μm. *E*, HeLa cells were treated with siRNA-p24 and immunostained with the antibody indicated on the *left*. Relative fluorescence intensity of proteins in either metaphase (*black bars*) or figure eight (*open bars*) centrosomes (*right panels*). The mean (+ S.D.) intensity of 50 centrosomal areas was measured, and background levels were subtracted. *Bar*, 5 μm. *Prometa*, prometaphase; *Meta*, metaphase; *Ana*, anaphase.

which 2.4% (4/163) underwent cell death. Moreover, the metaphase delay induced by siRNA-p150 (average 85 min, Fig. 4*C*, see Video 3) was more severe than in cells treated with siRNA-p24 and 6.7% (11/163) of siRNA-p150-treated mitotic cells underwent cell death during metaphase. These findings are consistent with previous experiments in which HeLa cells treated with siRNA-p150 showed increased ratios of cells in prometaphase and metaphase relative to cells in anaphase and telophase (Fig. 2*C*). Unlike cells treated with siRNA-p24, none of these mitotic cells showed chromosomes aligned in a figure eight pattern, and all cells that survived through prometaphase and metaphase entered anaphase.

Cells with Figure Eight Chromosome Alignment Share Features with Prometaphase—Our findings demonstrate that down-regulation of either p24 or $p150^{Glued}$ induces severe metaphasic delays. This phenotype is analogous to a previous report about cells that undergo metaphase arrest/delay when dynactin is depleted by dynamitin overexpression (8). In that case, the delay is most likely due to a defect in the function of the dynein-dynactin complex, which removes spindle checkpoint proteins such as BubR1 from kinetochores during metaphase (reviewed in Ref. 20). Indeed, when cells were treated with control siRNA, BubR1 signals localized to kinetochores in prometaphase (Fig. 5*A*, *panel 1*), after which the signal decreased rapidly during metaphase and anaphase (*panels 1* and *2*). In contrast, cells treated with siRNA-p24 showed the same intensity of BubR1 immunofluorescence at the kinetochores of metaphase chromosomes as that in prometaphase cells, including those cells with a figure eight chromosome alignment (*panel 3*).

Despite their similarities in appearance to prometaphase (rather than anaphase) cells, the figure eight chromosome alignment is only seen in cells that have progressed through metaphase (supplemental Movie 2). To further characterize the timing of this unique chromosomal alignment, we looked at expression of cyclin B1, a molecule that is present during metaphase (Fig. 5*B*, *Meta*) and then degraded rapidly in anaphase (*Ana*). We observed positive cyclin B1 immunofluorescence in all mitotic cells with a figure eight chromosome alignment. Moreover, FISH images of the c-*myc* gene on

Downloaded from www.jbc.org at HIROSHIMA UNIVERSITY, on February 15, 2011

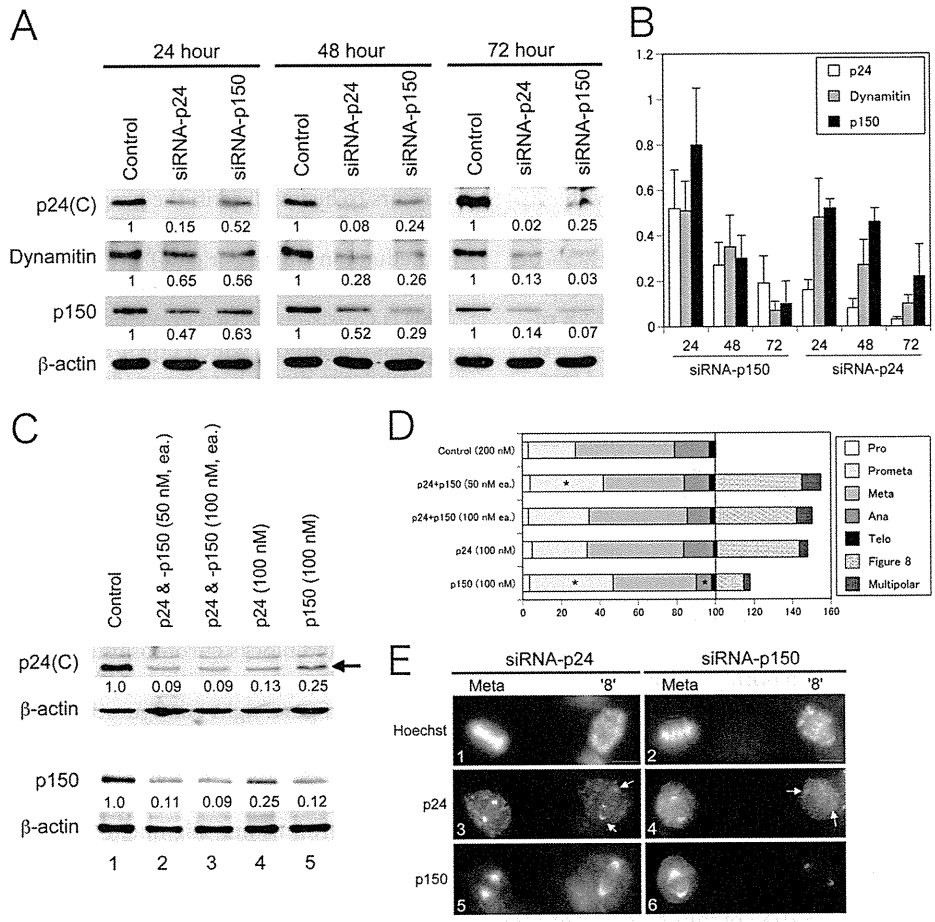

FIGURE 6. **p24 expression levels relate to figure eight configuration.** *A* and *C*, immunoblot analyses using p24(C), dynamitin, p150^{Glued}, or β-actin antibody. HeLa cells were treated with siRNA (100 nM, otherwise indicated) as indicated above for 72 h. Ratios of relative intensity (p24, dynamitin, or p150 actin) measured by densitometry are indicated *below each lane*. Data are representative of four independent experiments that yielded similar results. *B*, average and S.D. protein expression levels in four independent experiments of p24, dynamitin, and p150^{Glued} relative to control siRNA-treated cells. *D*, HeLa (tc) cells were treated with the siRNA indicated on the *left* for 72 h. From a total of 300 cells counted/treatment, the percentages of mitotic cells with normal-looking chromosome alignment (100% total) or abnormal mitosis were determined from observations of Hoechst 33342-stained nuclei. *Asterisks* indicate statistically significant changes in a particular mitotic phase ($p < 0.01$) relative to the no treatment control using a Chi-square test. *E*, HeLa cells were treated with the siRNA indicated above and immunostained with the antibody indicated on the *left*. DNA was stained with Hoechst 33342, and the mitotic phase of each cell is labeled *above*. *Bar*, 10 μm. *Pro*, prophase; *Prometa*, prometaphase; *Meta*, metaphase; *Ana*, anaphase; *Telo*, telophase. '8', figure eight.

chromosome band 8q24 indicate that sister chromatids in cells with figure eight alignment have yet to segregate because four pairs of dots are visible on chromosomes in figure eight cells (Fig. 5*C*, *arrows*; FISH with chromosome 8-specific centromeric probes revealed that HeLa(tc) cells have four chromosome 8 (data not shown)). These data suggest that cells with figure eight chromosome alignment are most like prometaphase cells.

Because the alignment of chromosomes on the metaphase plate is mediated by tension between the spindle poles, reversal of the mitotic process by siRNA-p24 interference may be due to reductions in spindle tension. Using α-tubulin immunostaining, we compared the density and morphology of spindles in cells at different stages of mitosis. In cells displaying a figure eight configuration (Fig. 5*D*, *panel 3*), the robust fluorescence characteristic of metaphase mitotic spindles (*panel 2*) reverted to a shape and intensity more characteristic of mitotic spindles in prometaphase (*panel 1*). Moreover, the marked decrease in immunostaining signal intensity for γ-tubulin and CG-NAP (pivotal components of the γ-tubulin ring complex that provides microtubule nucleation sites) in figure eight-stage cells relative to metaphase cells (Fig. 5*E*) suggests that p24 is required to maintain the integrity of metaphase centrosomes.

p24 Levels Relate to Figure Eight Chromosome Alignment—In parallel experiments conducted in two different cell lines (HeLa or U2OS), metaphase arrest/delay was induced similarly following treatment with either siRNA-p24 or siRNA-p150; however, siRNA-p24 was significantly more effective than siRNA-p150 in inducing the figure eight chromosome alignment during metaphase (Figs. 2*C* and 4, *B* and *C*). We did not observe any change in expression of p150^{Glued} and p24 mRNAs following treatment with siRNA-p24 or siRNA-p150, respectively (Fig. 1*A*). However, both of these siRNAs did reduce protein expression levels of p24, p150^{Glued}, and dynamitin in HeLa(tc) cells (Fig. 6*A*). Similar results were obtained in U2OS cells (data not shown). Similar to previous reports demonstrating that overexpression of dynamitin disrupts dynactin structure (2), our results with p24 and p150^{Glued} suggest that balanced availability of all

Downloaded from www.jbc.org at HIROSHIMA UNIVERSITY, on February 15, 2011